Phys Chem Minerals (2011) 38:139–157
DOI 10.1007/s00269-010-0390-3

ORIGINAL PAPER

Nuclear and incommensurate magnetic structure of $NaFeGe_2O_6$ between 5 K and 298 K and new data on multiferroic $NaFeSi_2O_6$

Günther J. Redhammer · Anatoliy Senyshyn · Martin Meven · Georg Roth · Sebastian Prinz · Astrid Pachler · Gerold Tippelt · Clemens Pietzonka · Werner Treutmann · Markus Hoelzel · Björn Pedersen · Georg Amthauer

Received: 9 April 2010 / Accepted: 20 July 2010 / Published online: 10 August 2010

Abstract The compound $NaFeGe_2O_6$ was grown synthetically as polycrystalline powder and as large single crystals suitable for X-ray and neutron-diffraction experiments to clarify the low temperature evolution of secondary structural parameters and to determine the low temperature magnetic spins structure. $NaFeGe_2O_6$ is isotypic to the clinopyroxene-type compound aegirine and adopts the typical H*T*-*C*2/*c* clinopyroxene structure down to 2.5 K. The Na-bearing M2 polyhedra were identified to show the largest volume expansion between 2.5 K and room temperature, while the GeO_4 tetrahedra behave as stiff units. Magnetic susceptibility measurements show a broad maximum around 33 K, which marks the onset of low-dimensional magnetic ordering. Below 12 K $NaFeGe_2O_6$ transforms to an incommensurately modulated magnetic spin state, with $\mathbf{k} = [0.323, 1.0, 0.080]$ and a helical order of spins within the M1-chains of FeO_6 octahedra. This is determined by neutron-diffraction experiments on a single crystal. Comparison of $NaFeGe_2O_6$ with $NaFeSi_2O_6$ is given and it is shown that the magnetic ordering in the latter compound, aegirine, also is complex and is best described by two different spin states, a commensurate one with $C2'/c'$ symmetry and an incommensurate one, best being described by a spin density wave, oriented within the (1 0 1) plane.

Keywords Clinopyroxene · $NaFeGe_2O_6$ · Aegirine $NaFeSi_2O_6$ · Multiferroic compounds · Neutron diffraction · Magnetic ordering · Helical spin structure

Electronic supplementary material The online version of this article (doi:10.1007/s00269-010-0390-3) contains supplementary material, which is available to authorized users.

G. J. Redhammer (✉) · A. Pachler · G. Tippelt · G. Amthauer
Abteilung für Mineralogie, Fachbereich Materialforschung und Physik, Universität Salzburg, Hellbrunnerstr. 34, 5020 Salzburg, Austria
e-mail: Guenther.redhammer@sbg.ac.at

A. Senyshyn · M. Meven · M. Hoelzel · B. Pedersen
Forschungneutronenquelle Heinz Maier-Leibnitz (FRM II), Lichtenbergstrasse 1, 85747 Garching, Germany

A. Senyshyn · M. Hoelzel
Fachgebiet Strukturforschung, Materialwissenschaft, Technische Universität Darmstadt, Petersenstr. 23, 64278 Darmstadt, Germany

G. Roth · S. Prinz
Institut für Kristallographie, RWTH Aachen, Jägerstraße 17/19, 52056 Aachen, Germany

C. Pietzonka
Fachbereich für Chemie, Philipps-University Marburg, Hans Meerweinstr, 35032 Marburg, Germany

W. Treutmann
Institut für Mineralogie, Philipps-University Marburg, Hans Meerweinstr, 35032 Marburg, Germany

Introduction

Clinopyroxene-type compounds ABT_2O_6 have been well known and studied in geoscience for decades, but have gained vivid interest in solid state physics in recent days due to their low temperature magnetic properties. Closely related compounds, such as $LiFeSi_2O_6$ and $LiFeGe_2O_6$, exhibit a variety of different magnetically ordered states (Redhammer et al. 2009). The overall bulk magnetic properties are determined by a competitive interplay between intra-chain and inter-chain coupling of the infinite M1 chains hosting the transition metal cations. Cr^{3+} based pyroxenes (Na, Li)Cr^{3+}(Si, Ge)$_2O_6$ are yet another good

examples for the richness of the magnetic ground states and on how M2 and T-site substitution alters the magnetic properties: $LiCrSi_2O_6$ is anti-ferromagnetic (Vasiliev et al. 2005, Nenert et al. 2009a), while $NaCrGe_2O_6$ displays ferromagnetic behaviour (Vasiliev et al. 2005, Nenert et al. 2009b). This diversity of the magnetic ground states is quite typical for transition metal ion-containing pyroxenes. To our current understanding ingredients contributing to this magnetic diversity are (1) almost 90° superexchange coupling within the chains of edge-sharing octahedra with a resulting ambiguity of even the sign of the strongest (intra-chain) interaction, (2) competing superexchange interactions via two different kinds of TO_4-tetrahedra (T = Si, Ge) and (3) an intrinsic structural instability towards a "kinking" of the tetrahedral chains which in turn modulates the superexchange interaction in a very delicate way.

The interest in pyroxenes additionally increased since Jodlauk et al. (2007) identified them as a new class of multiferroics, i.e. compounds with a combination of more than one ferroic property in either a single phase material or a multilayer heterostructure. $NaFeSi_2O_6$, $LiFeSi_2O_6$ and $LiCrSi_2O_6$ were presented to obey multiferroic behaviour and Jodlauk et al. (2007) discussed the possibility of incommensurate magnetic structures in these compositions due to magnetic frustration. Such a modulated magnetic structure, however, could not be confirmed in recent studies on $LiFeSi_2O_6$ (Redhammer et al. 2009) and $LiCrSi_2O_6$ (Nenert et al. 2009a). Both compounds display quite simple commensurate and collinear magnetic spin arrangements, at least at zero-external magnetic fields. On the contrary, aegirine $NaFeSi_2O_6$ indeed shows an incommensurate modulation of the magnetic structure at low temperatures (Ballet et al. 1989), the exact magnetic spin structure, however, remains to be determined. In this study, we report on the magnetic properties of the germanium analogue of aegirine, namely $NaFeGe_2O_6$.

This compound was first described by Solov'eva and Bakakin (1968) and was grown accidentally during hydrothermal crystallization in the Na_2O–MnO–GeO_2–H_2O system (with iron contributed by the Fe-lined pressure vessels). The authors found the compound to be isotypic to the pyroxene family, space group $C2/c$. No data are available for conditions other than ambient. The magnetic structure of $NaFeGe_2O_6$ also is not solved yet, even though some information is available from an ISIS Experimental Report (Behruzi et al. 1997): magnetic order appears to occur below 20 K where additional magnetic peaks arise in the neutron-diffraction pattern. Most of them could be indexed with a propagation vector $\mathbf{k} = 0, 0, 1/2$. However, it is reported that complete fits to the data could not be achieved (Behruzi et al. 1997). Drokina et al. (2008) reported an anti-ferromagnetic ordering temperature of 15 K and a paramagnetic Curie temperature of −135 K for a synthetic $NaFeGe_2O_6$ sample (with ∼5 wt% Fe_2O_3 as impurity). Drokina et al. (2008) concluded from their experiments that the inter-chain coupling is weak ($J \sim -0.07$ K), while the intra-chain cation–cation exchange integral is strongly negative with $J_1 \sim -11.5$ K, thus being clearly anti-ferromagnetic (Drokina et al. 2008).

Experimental

Material synthesis

A polycrystalline sample of $NaFeGe_2O_6$ was prepared by a solid-state ceramic sintering route in batches of ∼12 g. In a first step, mixtures of Na_2CO_3, Fe_2O_3 and GeO_2 in the exact stoichiometry of the desired compound were ground under ethanol, pressed into pellets, put into an open platinum crucible and fired under ambient pressure and oxygen fugacity at a temperature of 1,273 K. After a sintering time of 2 days, the sample material was reground, pressed and reheated, repeating this procedure five times to obtain a well crystalline single-phase polycrystalline powder.

Single crystals of the title compound were obtained from flux growth experiments using a mixture of Na_2MoO_4 and $NaVO_3$ as the high temperature solvent. One part of a stoichiometric oxide mixture of $NaFeGe_2O_6$ and 10 parts of the flux were slowly heated to 1473 K and held at this temperature for 48 h to allow the melt to homogenize. Afterwards temperature was lowered at a rate of 0.5 K/h to 973 K where the experiment was finished with the samples allowed to cool down in the furnace. Large brown, prismatic, pillar-like single crystals up to 5 mm in length and 2 mm in diameter were obtained; Fig. 1 shows exemplary crystals from one of these runs. For the sake of comparison, single crystals of aegirine $NaFeSi_2O_6$ were also grown by

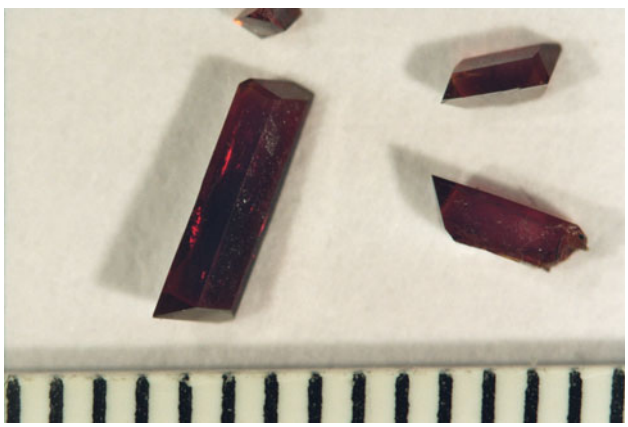

Fig. 1 Synthetic single crystals of $NaFeGe_2O_6$, obtained from flux growth experiments, one grid-line corresponds to 1 mm; the large crystal was used for single crystal neutron diffraction experiments

applying the same flux growth method outlined above. Crystals obtained are by far smaller than for $NaFeGe_2O_6$, have a brown–green colour and appear as tabular aggregates in sizes up to 250 μm.

SQUID magnetometry

The magnetic measurements were performed at the Philipps-University of Marburg/Lahn on a MPMS-2 SQUID-magnetometer (Quantum Design). Small amounts of sample material (between 30–40 mg) were put into polytrifluorethylen (KLF) containers and brought into measuring position using a straw. The variation of the magnetization as a function of temperature at fixed external magnetic field and as a function of the external field at fixed temperature was studied. A correction for the diamagnetism of the sample and the sample container was applied before calculating the susceptibilities from the magnetization data.

Powder X-ray diffraction

To obtain detailed information on the temperature variation of the lattice parameters, step-scan powder X-ray diffraction measurements (10° to 100° in 2Θ, continuous scan) were carried out in the temperature range 23–300 K at the Institute of Crystallography, RWTH Aachen, on a Philips X'Pert diffractometer ($CuK_{\alpha 1}$ radiation, fixed 0.125° divergence slit, primary and secondary 0.04 rad Soller slits, X'Celerator detector, Janis CCS-250 cryostat). High temperature data were collected also on a X'Pert diffractometer, using an Anton PAAR HTK-16 high temperature chamber and similar geometry and a conventional point detector. The FULLPROF-Suite of programs (Rodríguez-Carvajal 2001) was used for lattice parameter determination; however, no attempts were made to extract structural parameters from the X-ray powder diffraction data.

Single-crystal X-ray diffraction

Ten single-crystal X-ray diffraction experiments between 90 and 298 K, both on $NaFeGe_2O_6$ and $NaFeSi_2O_6$, were done on a Bruker SMART APEX CCD-diffractometer, equipped with a Bruker CRYOFLEX cryostat. Intensity data were collected with Mo Kα radiation (50 kV, 30 mA) and the detector positioned at $-28°$ 2Θ using a ω-scan mode strategy at four different ϕ positions. 630 frames with $\Delta\omega = 0.3°$ were acquired for each run. Three-dimensional data were integrated and corrected for Lorentz, polarization and background effects using the APEX2 software (Bruker-Nonius 2004). Structure solution (using Patterson methods) and subsequent refinement were carried out with the programs implemented in the program suite WinGX 1.64 (Farrugia 1999).

Neutron diffraction

Neutron-diffraction experiments were done at the Heinz Maier-Leibnitz Forschungsneutronenquelle (FRM II) Munich, Germany. Powder diffraction data were acquired in constant wavelength mode using the high resolution powder diffractometer SPODI (Hoelzel et al. 2007) on a ~10 g batch contained in a 14 mm diameter vanadium sample can at temperatures between 5 and 20.2 K with Ge331 monochromatized neutron radiation ($\lambda = 2.537$ Å). Experiments were performed in a 2θ range $3° \leq 2\theta \leq 145°$, step width 0.04°. Data treatment (**k** vector determination, Rietveld refinement) was done using the FULLPROF-suite of programs (Rodríguez-Carvajal 2001). The structural data obtained from the 100 K single X-ray crystal structure refinements were taken as starting parameters in Rietveld refinements.

To get a complete picture of the incommensurate modulation, single-crystal data up to 1.5 in $\sin\theta/\lambda$ were collected on the RESI diffractometer (= reciprocal space investigator with $\lambda = 1.474$ Å). Data evaluation was done using DIRAX (Duisenberg 1992) and the EVAL14 suite (Duisenberg et al. 2003). Single-crystal intensity data were collected at the HEiDi diffractometer at 2.5, 15 and 30 K with $\lambda = 0.87$ Å [Cu-(220) monochromator]. HEiDi is a four circle single-crystal diffractometer with an acentric Eulerian cradle using the high flux of hot neutrons at beam tube SR9A of the FRM II reactor. The closed cycle cryostat (Sumitomo SDK110) covers the temperature range between 2.5 K and room temperature within an error of less than 0.1 K at sample position.

A first data collection at 2.5 K up to $\sin\theta/\lambda = 0.3$ confirmed the C centering of the crystal structure at this temperature. For the full nuclear structure at this temperature, data acquisition was done up to $\sin\theta/\lambda = 0.8$ with about 2,200 Bragg reflections. A separate data set was collected for the incommensurately modulated magnetic reflections at $T = 2.5$ K up to $\sin\theta/\lambda = 0.6$ with $\mathbf{q} = \mathbf{k} = (0.323, 1.0, 0.080)$. The two Bragg data sets at 15 and 30 K were taken up to $\sin\theta/\lambda = 0.7$. An additional data set of selected magnetic and non-magnetic reflections was taken between 2.5 and 20 K to observe the thermal evolution of the incommensurate magnetic structure and determine the phase transition temperature which was found to be about 12.5 K.

Experimental data and refinement results of selected X-ray and neutron-diffraction measurements on $NaFeGe_2O_6$ and $NaFeSi_2O_6$ are compiled in Table 1, fractional atomic coordinates and isotropic atomic displacement parameters are listed in Table 2, while some secondary structural parameters are given in Table 3. The complete set of atomic coordinates and anisotropic displacement parameters for $NaFeGe_2O_6$ and also for $NaFeSi_2O_6$, at all

Table 1 Experimental details and results of structure refinements on single-crystal neutron and X-ray diffraction data for synthetic $NaFeGe_2O_6$ and $NaFeSi_2O_6$ at some selected temperatures

Sample	$NaFeGe_2O_6$						$NaFeSi_2O_6$		
Instr.	HEiDi			APEX			SPODI	APEX	
λ (Å)	0.87			0.7107			2.537	0.7107	
T (K)	2.5	15	30	110	200	298	5	90	190
a (Å)	9.9929(7)	9.9932(8)	9.9935(7)	9.9960(8)	10.0002(7)	10.0073(8)	9.6478(1)	9.6477(7)	9.6501(7)
b (Å)	8.9194(7)	8.9192(6)	8.9178(6)	8.9185(7)	8.9258(6)	8.9382(7)	8.7953(1)	8.7969(4)	8.8003(4)
c (Å)	5.5148(4)	5.5145(4)	5.5137(3)	5.5132(4)	5.5147(4)	5.5184(4)	5.2809(1)	5.2818(2)	5.2818(2)
β (°)	107.563(1)	107.552(1)	107.542(1)	107.539(1)	107.528(1)	107.524(1)	107.316(1)	107.318(4)	107.313(4)
V (Å^3)	468.63(6)	468.63(6)	468.53(6)	468.65(6)	469.39(6)	470.70(6)	427.80(3)	427.95(4)	428.23(4)
θ_{min} (°)	3.8	3.8	3.8	3.1	3.1	3.1	1.15	3.1	3.1
θ_{max} (°)	44.7	37.2	37.2	28.7	28.8	28.8	78.0	28.8	28.8
No refl.	1,035	662	659	575	578	580	–	530	532
R_{int} (%)	3.62	2.52	2.71	5.42	5.35	5.94	–	3.24	2.69
Range h	−16 to 15	−13 to 13	−13 to 13	−13 to 12	−13 to 12	−13 to 12	–	−12 to 12	−12 to 12
Range k	−14 to 14	−12 to 12	−12 to 12	−11 to 11	−11 to 11	−11 to 11	–	−11 to 11	−11 to 11
Range l	−3 to 8	−3 to 7	−3 to 7	−7 to 7	−7 to 7	−7 to 7	–	−7 to 7	−7 to 7
R_1 (%)	5.55	4.00	4.22	2.01	1.99	2.12	1.73	1.82	1.78
wR_2 (%)	7.17	5.47	5.56	4.92	4.73	4.82	–	4.73	4.71
R_{magn} (%)	6.39*	–	–	–	–	–	3.93, 6.65	–	–
Ext.	0.065	0.064	0.066	0.014	0.017	0.021	–	0.00.	0.002
$\Delta\rho_{max}$	1.22	1.14	1.12	0.87	0.94	1.05	–	0.30	0.33
$\Delta\rho_{min}$	−1.48	−0.93	−0.90	−1.03	−0.97	−1.00	–	−0.38	−0.42

The complete set of single-crystal data results (primary structural data) at 2.5, 15, 30, 110, 130, 150, 170, 190, 200, 230, 250 and 298 K for $NaFeGe_2O_6$ and at 90, 120, 160, 190, 220, 250 and 298 K for $NaFeSi_2O_6$ is available from the CIF-Files, which are deposited as supplementary items

All data; monoclinic cell setting, space group $C2/c$, $Z = 4$; refinement on F^2

* wR_2 value for magnetic structure only

Table 2 Fractional atomic coordinates, anisotropic and equivalent isotropic atomic displacement parameters for $NaFeGe_2O_6$ and $NaFeSi_2O_6$ at selected temperatures, as extracted from single-crystal neutron and X-ray diffraction data

Atom	x	y	z	U_{11}	U_{22}	U_{33}	U_{23}	U_{13}	U_{12}	U_{eq}
$NaFeGe_2O_6$										
$T = 298$ K										
Na1	0	0.3008(2)	0.25	0.0162(8)	0.0104(8)	0.0140(8)	0	0.0003(5)	0	0.015(5)
Fe1	0	0.90359(4)	0.25	0.0045(3)	0.0050(3)	0.0056(3)	0	0.0013(2)	0	0.0051(2)
Ge1	0.28802(2)	0.09388(2)	0.22857(4)	0.0042(2)	0.0054(2)	0.0057(2)	−0.00032(7)	0.00168(6)	−0.0006(2)	0.00510(2)
O1	0.1056(2)	0.0804(2)	0.1307(3)	0.0048(7)	0.0080(7)	0.0066(8)	−0.00018(5)	0.0007(7)	−0.0008(5)	0.0067(4)
O2	0.3570(2)	0.2713(2)	0.2983(3)	0.0108(8)	0.0079(8)	0.0138(8)	−0.0021(6)	0.0050(6)	−0.0041(6)	0.0106(3)
O3	0.3610(1)	0.0065(2)	0.0140(3)	0.0071(8)	0.0128(9)	0.0090(8)	−0.0036(6)	0.0020(6)	0.0004(6)	0.0096(4)
$T = 200$ K										
Na1	0	0.3009(2)	0.25	0.0114(8)	0.00806(7)	0.0114(8)	0	0.0014(6)	0	0.011(4)
Fe1	0	0.90376(4)	0.25	0.0028(3)	0.0037(3)	0.0050(3)	0	0.0013(2)	0	0.0038(2)
Ge1	0.28809(2)	0.09395(2)	0.22916(5)	0.0029(2)	0.0039(3)	0.0051(3)	−0.0002(7)	0.0015(3)	−0.0004	0.0039(2)
O1	0.1053(2)	0.0808(2)	0.1305(3)	0.0041(8)	0.0050(8)	0.0064(8)	−0.0001(6)	0.0014(7)	−0.0007	0.0052(4)
O2	0.3570(2)	0.2718(2)	0.2996(3)	0.0081(7)	0.0068(7)	0.0107(8)	−0.0015(6)	0.0036(6)	−0.0030	0.0083(4)
O3	0.3614(2)	0.0069(2)	0.0143(3)	0.0047(8)	0.0098(8)	0.0076(7)	−0.0030(7)	0.0017(6)	0.0005	0.0074(5)

Table 2 continued

Atom	x	y	z	U_{11}	U_{22}	U_{33}	U_{23}	U_{13}	U_{12}	U_{eq}
$T = 110$ K										
Na1	0	0.3008(2)	0.25	0.0074(7)	0.0056(6)	0.0078(6)	0	0.0016(6)	0	0.0071(5)
Fe1	0	0.90386(5)	0.25	0.0016(3)	0.0025(3)	0.0039(3)	0	0.0013(2)	0	0.0026(2)
Ge1	0.28808(3)	0.09398(3)	0.22957(6)	0.0022(2)	0.0028(3)	0.0043(3)	−0.0001(6)	0.0014(2)	−0.0002(6)	0.0030(2)
O1	0.1052(2)	0.0810(2)	0.1308(2)	0.0028(7)	0.0042(7)	0.0060(7)	−0.0005(6)	0.0010(6)	−0.0008(7)	0.0044(4)
O2	0.3571(2)	0.2720(2)	0.3005(3)	0.0075(7)	0.0049(6)	0.0086(7)	−0.0014(7)	0.0036(7)	−0.0028(6)	0.0067(3)
O3	0.3616(2)	0.0072(2)	0.0145(2)	0.0039(7)	0.0068(7)	0.0060(7)	−0.0023(6)	0.0018(6)	0.0002(7)	0.0055(4)
$T = 30$ K										
Na1	0	0.3003(4)	0.25	0.0051(10)	0.0024(11)	0.0032(13)	0	0.0020(12)	0	0.0034(12)
Fe1	0	0.9039(1)	0.25	0.0013(5)	0.0015(5)	0.0025(5)	0	0.0003(3)	0	0.0018(5)
Ge1	0.2881(2)	0.0940(2)	0.2298(2)	0.0017(4)	0.0020(4)	0.0015(4)	0.0001(4)	0.0005(3)	−0.0007(4)	0.0017(4)
O1	0.1053(2)	0.0805(2)	0.1303(2)	0.0020(4)	0.0021(4)	0.0029(5)	0.0007(5)	−0.0004(3))	−0.0011(3)	0.0026(4)
O2	0.3569(2)	0.2717(2)	0.2996(2)	0.0033(4)	0.0029(5)	0.0062(5)	−0.0011(4)	0.0023(4)	−0.0016(4)	0.0039(5)
O3	0.3616(2)	0.0071(2)	0.0143(2)	0.0032(5)	0.0043(4)	0.0032(5)	−0.0009(4)	0.0014(3)	−0.0001(4)	0.0035(4)
$T = 15$ K										
Na1	0	0.3000(4)	0.25	0.0060(11)	0.0025(11)	0.0032(14)	0	0.0024(12)	0	0.0037(11)
Fe1	0	0.9038(1)	0.25	0.0012(5)	0.0017(4)	0.0027(6)	0	0.0003(3)	0	0.0019(4)
Ge1	0.2881(2)	0.0938(1)	0.2296(2)	0.0021(5)	0.0020(5)	0.0017(5)	0.0000(4)	0.0008(3)	−0.0006(3)	0.0019(3)
O1	0.1053(3)	0.0803(2)	0.1304(2)	0.0018(6)	0.0024(4)	0.0036(5)	0.0004(5)	−0.0002(4)	−0.0011(4)	0.0028(3)
O2	0.3569(2)	0.2717(1)	0.2997(2)	0.0038(5)	0.0027(4)	0.0067(4)	−0.0007(4)	0.0023(4)	−0.0015(4)	0.0043(4)
O3	0.3615(2)	0.0070(2)	0.0149(2)	0.0033(4)	0.0043(5)	0.0029(4)	−0.0015(4)	0.0013(4)	−0.0004(4)	0.0034(3)
$T = 2.5$ K										
Na1	0	0.3004(4)	0.25	0.0055(12)	0.0049(12)	0.0059(16)	0	0.0012(11)	0	0.0052(12)
Fe1	0	0.9038(1)	0.25	0.0003(5)	0.0005(5)	0.0024(6)	0	0.0001(3)	0	0.0011(4)
Ge1	0.2881(2)	0.0939(1)	0.2299(2)	0.0008(4)	0.0012(4)	0.0011(4)	−0.0004(4)	0.0008(3)	−0.0003(3)	0.0009(3)
O1	0.1053(2)	0.0807(2)	0.1303(3)	0.0015(5)	0.0019(5)	0.0029(6)	0.0005(4)	0.0004(4)	−0.0010(4)	0.0022(3)
O2	0.3567(2)	0.2715(2)	0.2995(2)	0.0026(6)	0.0018(4)	0.0056(4)	−0.0007(3)	0.0022(4)	−0.0017(4)	0.0031(3)
O3	0.3616(2)	0.0070(2)	0.0147(2)	0.0017(5)	0.0043(4)	0.0029(4)	−0.0014(4)	0.0014(4)	−0.0000(3)	0.0028(3)
$NaFeSi_2O_6$										
$T = 5$ K										
Na1	0	0.3015(5)	0.25	–	–	–	–	–	–	0.0118(14)
Fe1	0	0.8991(2)	0.25	–	–	–	–	–	–	0.0072(7)
Si1	0.2894(2)	0.0900(4)	0.2343(5)	–	–	–	–	–	–	0.0027(7)
O1	0.1139(2)	0.0788(3)	0.1376(4)	–	–	–	–	–	–	0.0114(7)
O2	0.3599(2)	0.2579(2)	0.3009(4)	–	–	–	–	–	–	0.0100(7)
O3	0.3530(3)	0.0085(2)	0.0112(6)	–	–	–	–	–	–	0.0129(7)
$T = 90$ K										
Na1	0	0.29969(11)	0.25	0.0094(6)	0.0061(6)	0.0064(6)	0	0.0007(4)	0	0.0076(4)
Fe1	0	0.89950(4)	0.25	0.0042(2)	0.0036(2)	0.0032(2)	0	0.0012(1)	0	0.0037(2)
Si1	0.29069(5)	0.08983(5)	0.23520(9)	0.0058(3)	0.0049(3)	0.0052(3)	−0.0002(2)	0.0019(2)	−0.0001(2)	0.0052(2)
O1	0.1140(2)	0.0787(1)	0.1379(3)	0.0080(7)	0.0078(6)	0.0059(6)	−0.0001(4)	0.0026(5)	−0.0002(5)	0.0071(3)
O2	0.3584(1)	0.2567(1)	0.3010(2)	0.0089(7)	0.0076(6)	0.0078(6)	0.0000(5)	0.0030(5)	−0.0003(5)	0.0080(3)
O3	0.3525(1)	0.0079(2)	0.0123(2)	0.0082(7)	0.0084(6)	0.0071(6)	−0.0004(5)	0.0025(5)	0.0008(5)	0.0078(3)
$T = 190$ K										
Na1	0	0.2998(1)	0.25	0.0132(6)	0.0077(5)	0.0089(5)	0	−0.000(4)	0	0.0107(4)
Fe1	0	0.89930(3)	0.25	0.0051(2)	0.0048(2)	0.0045(2)	0	0.0014(1)	0	0.0048(2)
Si1	0.29066(5)	0.08982(5)	0.23495(9)	0.0057(3)	0.0060(3)	0.0060(3)	−0.0003(1)	0.0019(2)	−0.0002(2)	0.0059(2)
O1	0.1139(2)	0.0785(1)	0.1377(2)	0.0080(6)	0.0091(6)	0.0073(6)	0.0004(4)	0.0026(4)	−0.0001(4)	0.0081(3)
O2	0.3585(1)	0.2565(1)	0.3007(2)	0.0098(6)	0.0089(6)	0.0099(6)	0.0002(4)	0.0033(4)	−0.0009(4)	0.0095(3)
O3	0.3523(1)	0.0077(1)	0.0120(2)	0.0093(6)	0.0093(6)	0.0090(6)	−0.0010(4)	0.0029(5)	0.0011(4)	0.0091(3)

Table 3 Selected bond lengths (Å), angles (°) and distortional parameters for $NaFeGe_2O_6$ and $NaFeSi_2O_6$ at some selected temperatures, as extracted from neutron and X-ray diffraction data

	$NaFeGe_2O_6$						$NaFeSi_2O_6$		
T (K)	2.5	15.0	30.0	110	200	298	5	90	190
Fe–O2	1.936(1)	1.936(1)	1.935(1)	1.935(1)	1.933(1)	1.936(1)	1.913(2)	1.932(1)	1.932(1)
Fe–O1	2.049(1)	2.049(1)	2.048(1)	2.050(1)	2.051(1)	2.053(1)	2.024(4)	2.026(1)	2.025(1)
Fe–O1	2.107(1)	2.107(1)	2.108(1)	2.109(1)	2.111(1)	2.114(1)	2.109(3)	2.105(1)	2.106(1)
<Fe–O>Å	*2.030*	*2.030*	*2.030*	*2.031*	*2.032*	*2.034*	*2.016*	*2.021*	*2.021*
Vol_{M1}	10.83	10.83	10.83	10.85	10.85	10.90	10.73	10.81	10.81
OAV	67.02	67.14	66.83	66.76	66.76	65.63	41.62	40.95	41.37
$[Fe–Fe]_{inter}$	3.247(1)	3.247(1)	3.246(1)	3.247(1)	3.249(1)	3.253(1)	3.185(1)	3.178(1)	3.181(1)
$[Fe–Fe]_{intra}$	5.638(1)	5.638(1)	5.639(1)	5.640(1)	5.642(1)	5.646(1)	5.435(1)	5.439(1)	5.438(1)
Fe–O1–Fe	102.78(4)	102.79(4)	102.74(4)	102.62(5)	102.68(5)	102.66(4)	100.67(9)	100.58(5)	100.67(6)
Na–O1	2.410(2)	2.407(2)	2.410(2)	2.408(2)	2.412(2)	2.420(2)	2.405(4)	2.393(2)	2.396(2)
Na–O2	2.546(2)	2.545(2)	2.546(2)	2.543(2)	2.549(2)	2.555(2)	2.412(4)	2.410(1)	2.411(1)
Na–O3	2.431(2)	2.434(2)	2.432(2)	2.430(2)	2.431(2)	2.433(2)	2.419(4)	2.428(1)	2.428(1)
Na–O3	2.870(2)	2.870(2)	2.864(2)	2.861(2)	2.865(2)	2.871(2)	2.806(4)	2.826(2)	2.826(2)
<Na–O>	2.564	2.564	2.563	2.561	2.564	2.570	2.511	2.514	2.515
Vol_{M2}	27.72	27.72	27.68	27.63	27.73	27.90	26.07	26.14	26.16
T–O1	1.745(1)	1.746(1)	1.746(1)	1.747(1)	1.747(1)	1.744(1)	1.620(3)	1.631(2)	1.631(1)
T–O2	1.726(1)	1.726(1)	1.724(1)	1.728(1)	1.728(1)	1.726(1)	1.620(3)	1.603(1)	1.602(1)
T–O3	1.750(1)	1.751(1)	1.755(1)	1.752(1)	1.752(1)	1.751(1)	1.646(4)	1.637(1)	1.637(1)
T–O3	1.768(1)	1.768(1)	1.766(1)	1.768(1)	1.768(1)	1.769(1)	1.653(4)	1.648(1)	1.647(1)
<T–O>	1.747	1.748	1.748	1.749	1.749	1.747	1.635	1.630	1.629
Vol_T	2.71	2.71	2.72	2.72	2.72	2.71	2.23	2.21	2.209
TAV	24.65	24.67	24.76	24.57	24.76	24.78	16.96	13.97	14.12
T–O3–T	132.92(6)	132.90(6)	132.85(5)	132.82(7)	132.96(7)	133.15(7)	137.9(2)	139.09(7)	139.14(7)
O3–O3–O3	185.07(5)	185.14(5)	185.24(5)	185.35(5)	185.13(5)	184.84(5)	173.5(1)	173.99(5)	174.09(5)

$OAV = \sum_{i=1}^{12} (\Theta_i - 90°)^2 \Big/ 11$ with Θ_i = O–M–O bonding angle (Robinson et al. 1971)

$TAV = \sum_{i=1}^{6} (\Theta_i - 109.57°)^2 \Big/ 5$ with Θ_i = O–T–O bonding angle (Robinson et al. 1971)

temperatures is available from the crystallographic information files (CIFs), which are deposited as supplementary material, also a list of lattice parameters at all temperatures is deposited.

Results and discussion

Nuclear structure of $NaFeGe_2O_6$ at 298 K

$NaFeGe_2O_6$ has monoclinic symmetry at 298 K, space group *C*2/*c*, *Z* = 4. Among the $AFe^{3+}T_2O_6$ (A = Na, Li; T = Si, Ge) clinopyroxenes, $NaFeGe_2O_6$ exhibits the largest unit cell parameters *a, b*, *c*, and the largest unit cell volume. The crystal structure contains one distinct M1 site, occupied by Fe^{3+}, one distinct M2 site, occupied by Na^+ (both Wykoff position 4*e*, site symmetry 2), one T-site hosting the Ge^{4+} cation and three independent oxygen atom sites O1–O3, all on general position 8*f* with site symmetry 1. The structure of $NaFeGe_2O_6$ is consistent with the well known H*T*-*C*2/*c* clinopyroxene structure type. It consists of infinite chains of edge-sharing M1-octahedra, running parallel the crystallographic *c* axis. These M1-chains are bridged by GeO_4 tetrahedra, which in turn form infinite kinked chains along *c* by corner sharing. Sodium occupies the irregularly shaped 6 + 2 fold coordinated M2 site, which is attached to the M1 polyhedra (Fig. 2).

The average $<Fe^{3+}–O>$ distance at M1 in $NaFeGe_2O_6$ is 2.034(2) Å, being the longest among the $AFe^{3+}T_2O_6$ (A = Na, Li; T = Si, Ge) clinopyroxenes at 298 K. Compared to aegirine, this is mainly due to a stretching of the short Fe–O1 bond, pointing along the **c**-direction. This represents an effective mechanism to sustain the matching of octahedral and tetrahedral chains. The longer Fe–O1, and the Fe–O2 bonds remain similar in the silicate and the germanate compounds (Table 4). The polyhedral volume of the M1 octahedron in $NaFeGe_2O_6$ is slightly larger compared to aegirine, but the M1 site suffers substantial distortion in the germanate with large values of the octahedral angle variance (OAV) and the quadratic octahedral

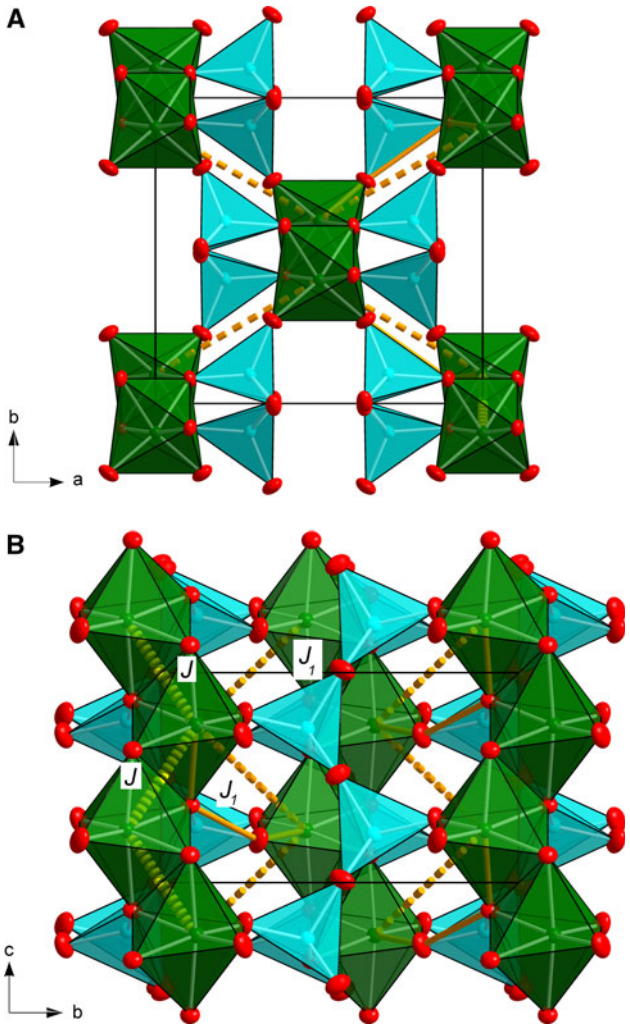

Fig. 2 Diagram of the crystal structure of $NaFeGe_2O_6$ at 30 K, extracted from single crystal neutron diffraction data; possible magnetic exchange interactions *J* are marked: **a** in a view onto the **a**–**b** plane, **b** in a view onto the **a**–**c** plane

elongation (QOE) due to the elongation along *c*. The OAV in $NaFeGe_2O_6$ is significantly larger (65.63 at 298 K), both compared to aegirine (41.47at 298 K) and also $LiFeGe_2O_6$ (50.51 at 298 K), which, however, exhibits $P2_1/c$ symmetry at 298 K. The substitution of Si^{4+} by Ge^{4+} in the tetrahedral chain of the alkali-iron pyroxenes thus introduces a distinct polyhedral distortion, which is large in the H*T*-*C*2/*c* structure, but can be reduced by lowering the symmetry to $P2_1/c$. For example, the OAV is reduced from 66.11 to 50.85 upon the $P2_1/c \leftrightarrow C2/c$ phase transition in $LiFeGe_2O_6$ (Redhammer et al. 2010b). Topological key data with respect to magnetic spin structures of pyroxenes are the intra- and inter-chain distances and superexchange M–O–M angles. Within the M1 chain, magnetic superexchange takes place along *J* (Fig. 2b) via the O1 oxygen atom: the shortest Fe–$Fe_{(inter)}$ contact between neighbouring Fe^{3+} atoms is 3.253(1), the Fe–O1–Fe angle amounts

Table 4 Comparison of selected structural and distortional parameters in *C*2/*c* (Na,Li)$Fe^{3+}(Si,Ge)_2O_6$ pyroxenene compounds

	$NaFeGe_2O_6^{\$}$	$NaFeSi_2O_6^{\$}$	$LiFeGe_2O_6^{\S}$	$LiFeSi_2O_6^{\&}$
T (K)	298	298	810	298
a (Å)	10.0073(8)	9.65557()	10.0963(7)	9.6641(8)
b (Å)	8.9382(7)	8.8094(7)	8.7239(5)	8.6602(8)
c (Å)	5.5184(4)	5.2843(4)	5.5341(4)	5.2924(4)
β (°)	107.524(1)	107.308(1)	109.839(6)	110.12(2)
Fe–O1	2.114(1)	2.112(2)	2.113(5)	2.133(1)
Fe–O1	2.053(1)	2.026(2)	2.081(6)	2.029(1)
Fe–O2	1.936(1)	1.933(2)	1.898(6)	1.912(1)
<Fe–O>	2.034	2.0234	2.031	2.0247
Vol_{M1}	10.90	10.85	10.84	10.87
OAV	65.63	41.47	66.11	41.77
OQE	1.0210	1.0134	1.0222	1.0142
Fe–Fe	3.253(1)	3.185(1)	3.236(2)	3.179(1)
Fe–Fe	5.646(1)	5.441(1)	5.556(2)	5.304(1)
Fe–O–Fe	102.66(4)	100.64(4)	100.9(2)	99.55(5)
T–O1	1.744(1)	1.628(2)	1.747(6)	1.634(1)
T–O2	1.726(1)	1.603(2)	1.709(6)	1.597(1)
T–O3	1.751(1)	1.638(2)	1.752(5)	1.623(1)
T–O3	1.769(1)	1.647(2)	1.752(6)	1.629(1)
<T–O>	1.747	1.629	1.740	1.621
Vol_T	2.71	2.21	2.67	2.18
TAV	24.78	14.35	26.07	10.98
TQE	1.0061	1.0034	1.0071	1.0028
Tau	112.92(5)	111.08(5)	112.5(2)	110.76(7)
O3–O3–O3	184.84(5)	185.87(6)	194.7(2)	180.98(8)
T–O–T	133.15(7)	139.216(5)	132.4(3)	141.15(8)
M2–O1	2.420(2)	2.400(2)	2.179(19)	2.081(2)
M2–O2	2.555(2)	2.414(2)	2.499(9)	2.181(2)
M2–O3	2.433(2)	2.432(2)	2.255(19)	2.488(2)
M2–O3	2.871(2)	2.830(2)	–	–
<M2–O>	2.570	2.519	2.311	2.250
Vol_{M2}	27.90	26.28	12.10	11.24

Bond lengths are given in (Å), volume in ($Å^3$) and OAV. TAV is given in (°). TQE and OQE are dimensionless. Polyhedral volumes were calculated using the program XTALDRAW (Downs 2005)

$ this study

§ Redhammer et al. (2010a, b)

& Redhammer et al. (2001)

$OAV = \sum_{i=1}^{12} (\Theta_i - 90°)^2 / 11$ with Θ_i = O–M–O bonding angle (Robinson et al. 1971)

$OQE = \sum_{i=1}^{6} (l_i/l_o)^2 / 6$ where l_o = central to vertex distance for a regular octahedron whose volume is equal to that of the undistorted tetrahedron with bond length l_i (Robinson et al. 1971)

$TAV = \sum_{i=1}^{6} (\Theta_i - 109.57°)^2 / 5$ with Θ_i = O–T–O bonding angle (Robinson et al. 1971)

$TQE = \sum_{i=1}^{4} (l_i/l_0)^2 / 4$ where l_o = central to vertex distance for a regular tetrahedron whose volume is equal to that of the undistorted octahedron with bond length l_i (Robinson et al. 1971)

102.65(7)°. Among all the Fe^{3+} bearing alkali-pyroxenes, this is by far the largest separation between neighbouring M1 sites within the chain and the most distinct deviation from an ideal 90° M–O–M bonding topology, that would favour ferromagnetic (FM) coupling of magnetic spins (Redhammer et al. 2009). For comparison, $LiFeSi_2O_6$ in the $P2_1/c$ low temperature phase has Fe–O1–Fe angles of 97.7° and 99.1° and FM coupling of the spins (data for 1.4 K), while the $LiFeGe_2O6$ clinopyroxene with Fe–O1–Fe angles of 100.4° and 101.6° already exhibits an antiferromagnetic (AFM) superexchange interaction within the M1 chain (data at 5 K), allowing to postulate a critical Fe–O–Fe angle of ~95–98° where the intra-chain interaction changes from FM to AFM (Redhammer et al. 2009, Streltsov and Khomskii 2008). Thus, the structural topology in $NaFeGe_2O_6$, but also the one in aegirine (Table 4), suggests assuming an AFM coupling of spins within the chains of $Fe^{3+}O_6$ octahedra at low temperatures. The interaction of neighbouring M1 chains involves the tetrahedral chains. The shortest distance between Fe atoms in different chains (interaction J_1 in Fig. 2) is 5.646(1) Å, which again is the largest separation among the Fe^{3+} bearing pyroxenes: in aegirine, the Fe–Fe separation in different chains is 5.441(1) Å only, in $LiFeSi_2O_6$ it is 5.304(1) Å. Connected to this also the super-exchange paths involving the tetrahedron (whether via the edge or involving the covalency of the tetrahedral cation also) is much longer in $NaFeGe_2O_6$ compared to the other compounds mentioned.

In the iron-bearing sodium pyroxenes, the M2 site has 6 + 2 fold coordination. Six Na–O bonds lie between 2.40 and 2.55 Å, the two remaining, but symmetry equivalent bonds are 2.871(3) and 2.830(3) Å in $NaFeGe_2O_6$ and $NaFeSi_2O_6$, respectively. Generally, all Na–O bond lengths are larger in $NaFeGe_2O_6$ compared to the silicate. This is most evident for the bonds to the O2 atoms (Table 4), reflecting distinctly the stretching of the unit cell in **c**-direction due to the increased size of the tetrahedral chain. The stretching of Na–O bonds is also displayed in larger <Na–O> bonds and a larger polyhedral volume in $NaFeGe_2O_6$.

The replacement of Si^{4+} by Ge^{4+} increases the average T–O bond lengths by ~0.12 Å to a value of 1.748(2) Å in $NaFeGe_2O_6$. This increase corresponds well to the difference of 0.13 Å in ionic radii of Si^{4+} and Ge^{4+} in tetrahedral coordination. The enlargement of the *c*-lattice dimension in $NaFeGe_2O_6$ relative to aegirine can directly be related to the Si^{4+} by Ge^{4+} substitution. Average <Ge–O> distances in $NaFeGe_2O_6$ are similar to those in $LiFeGe_2O_6$, both in the $P2_1/c$ and the $C2/c$ modification, as are the tetrahedral distortion parameters among the germanates. However, it is evident that the tetrahedra in $NaFeGe_2O_6$ exhibit a larger angular distortion and are more stretched towards the apical O1 oxygen atom than the ones in the silicate aegirine. The infinite tetrahedral chain in $NaFeGe_2O_6$ is S-rotated and almost stretched with the tetrahedral bridging angle O3–O3–O3 being 184.84(5)°, thus having a different kinking state as in aegirine, which is O-rotated (Table 4). This change in rotational sense obviously helps to account for the larger tetrahedra. Additionally, the T–O–T angle is decreased from 139.21(5)° in $NaFeSi_2O_6$ to 133.15(5)° in $NaFeGe_2O_6$. Thereby the O3–O3 edge length of the tetrahedral base plane is reduced and shows the smallest increase of all tetrahedral O–O edges when going from $NaFeSi_2O_6$ to $NaFeGe_2O_6$ (+0.116 Å or 4.2%), while the other edges increase by 6.6–8.5%. So edge lengths and O–T–O and T–O–T bond angle alterations become active also to maintain the match between octahedral and tetrahedral chains.

Temperature evolution of the nuclear structure

The nuclear structure of $NaFeGe_2O_6$ retains $C2/c$ symmetry down to 2.5 K. In the single-crystal neutron-diffraction experiments at 2.5, 15 and 30 K, no evidences were found for any Bragg reflections violating the *C*-centring. The variation of lattice parameters with temperature is shown in Fig. 3. Above room temperature (298 K), *a*, *b* and *c* increase almost linearly with temperature, while below ~200 K low-temperature saturation takes place. With the exception of the monoclinic angle β, data above 50 K were successfully fitted to a simple quasi-harmonic Einstein model to extract thermal expansion coefficients, the method being described in detail in recent papers (Redhammer et al. 2009, 2010a, b). Below 298 K, the shortening of the *b* axis is most pronounced, while the *c* axis exhibits only minor shrinking (Fig. 3f), indicating that the stiff tetrahedral chain hampers the thermal expansion, especially at low temperature. This behaviour continues at higher temperatures and leads to a linear thermal expansion coefficients of 8.5×10^{-6}, 13.2×10^{-6} and 7.0×10^{-6} K^{-1} for the *a*, *b* and *c* unit cell dimensions, respectively, showing the *b* axis to be most expansible. Redhammer et al. (2010b) give a more detailed discussion on the thermal expansion coefficients in $NaFeGe_2O_6$ with comparison to other pyroxenes, this discussion therefore will not be repeated here. From the fits of the simple quasi-harmonic Einstein model, saturation temperatures θ_E of 409(6), 311(7) and 478(11) K were extracted for *a*-, *b*- and *c*-lattice parameters, constituting the temperature above which a constant linear thermal expansion is observed; the unit cell volume shows constant expansion above 369(6) K. Very similar behaviour is found for aegirine (powder sample AcF2f, Redhammer et al. 2000), exhibiting higher saturation temperatures θ_E of 484(16), 426(15), and 661(21) K for *a*, *b* and *c*, respectively, but smaller

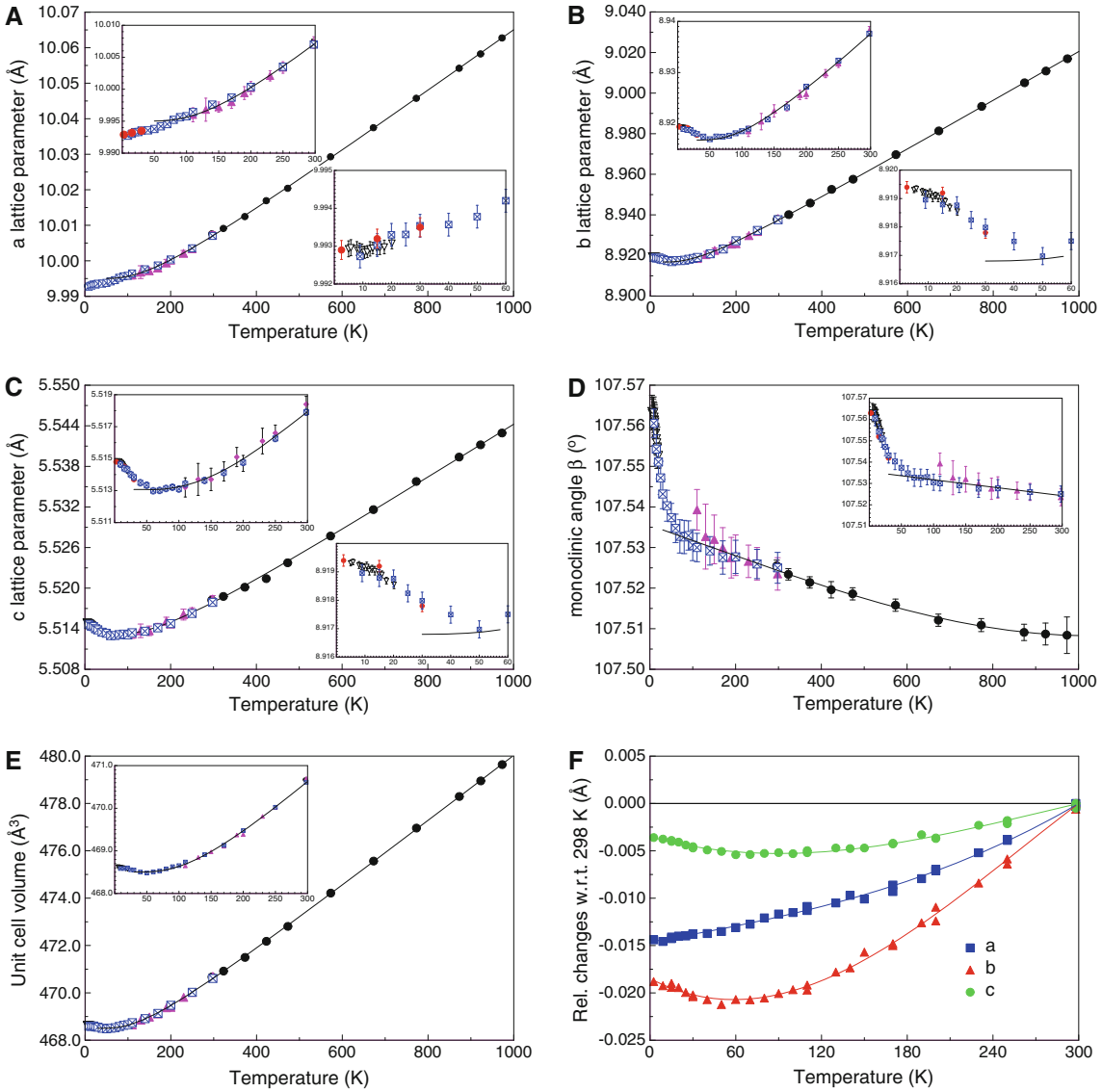

Fig. 3 Variation of lattice parameters with temperature in $NaFeGe_2O_6$ between 2.5 and 973 K. The *insets* show the low temperature ranges on enlarged scales. *Black solid dots* high temperature X-ray powder diffraction data (Salzburg), *blue open crossed squares* low temperature X-ray powder diffraction data (Aachen), *magenta filled triangles* X-ray single-crystal data (APEX), *red filled dots* single crystal neutron diffraction data (HEiDi), *open black triangles* Neutron powder diffraction data (SPODI)

thermal expansion coefficient, consistent with the general observation that germanate pyroxene compounds show a larger thermal expansion than the analogous silicates (Redhammer et al. 2010b).

Below 50 K, the *b*- and *c*-lattice parameters and the monoclinic angles increase again, i.e. a negative thermal expansion is observed, while the **a**-direction still decreases while cooling and no low temperature saturation is observed as normally would be expected (insets in Fig. 3). The monoclinic angle exhibits a distinctly larger increase below ~100 K compared to the steady variation above this temperature. The low temperature alterations of lattice parameters are related to the magnetic ordering in the compound. However, no sharp discontinuities are found in $NaFeGe_2O_6$ as observed e.g. in the Ca-pyroxenes (Redhammer et al. 2008). Additionally these deviations from the expected low temperature variation with saturation takes place tenths of K above the 3D magnetic ordering of the sample, suggesting that low-dimensional ordering or pre-ordering phenomena occur in $NaFeGe_2O_6$. These magnetostriction effects found here are by far not as pronounced as e.g. in the silicates: while in $LiFeSi_2O_6$ several non linear variations in interatomic distances and angle occur throughout the magnetic phase transition, they are weak in the analogue germanate $LiFeGe_2O_6$ (Redhammer et al. 2009). The same observation is made here for the aegirine–germanate compared to the silicate. Obviously, the strong magneto-elastic coupling that is a distinct feature

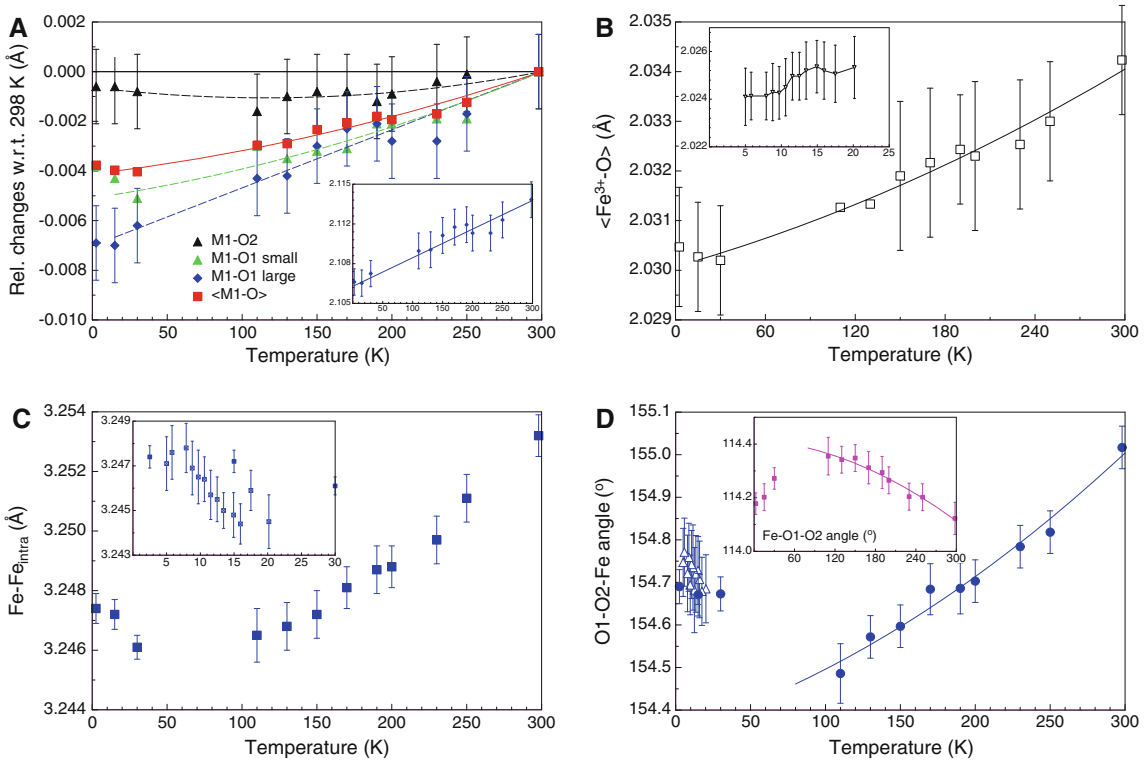

Fig. 4 Variation of secondary structural parameters at the M1 site with temperature for $NaFeGe_2O_6$: **a** relative changes of individual and average Fe–O bonds with respect to their room temperature values, the *inset* displays the absolute values for the larger Fe–O1 bond lengths; **b** absolute values for the <Fe–O> bonds, the *inset* shows the low T values obtained from Rietveld refinements of powder data; **c** variations in the Fe–Fe separation within the M1 chain and **d** variations of Fe–O1–O2 and O1–O2–Fe super-exchange angles between two neighbouring M1 chains; *curves* fitted to the data are guides to the eye only

of the multiferroic silicate pyroxenes is much less pronounced in the isotypic germanates.

Secondary structural parameters, extracted from single-crystal X-ray and neutron-diffraction data between 2.5 K and room temperature, show small variations with temperature. Among the individual M1–O bond lengths it is the longer Fe–O1, pointing towards the **b**-direction, which decreases most with temperature (~0.008 Å between 15 and 300 K, Fig. 4a), while the Fe–O2 bonds, directed towards the b axis, remain almost constant. The <Fe–O> decreases steadily with decreasing T, additionally, the low temperature (5–20 K) data obtained from the Rietveld refinements on the neutron-diffraction powder data suggest some very weak shrinking of the average Fe–O bond lengths due to a magneto-elastic coupling (inset in Fig. 4b). These small changes are not resolved in the single crystal data, but are visible especially in the individual Fe–O2 and short Fe–O1 bond lengths in the 5–22 K Rietveld data.

With decreasing temperature, the volume of the M1 polyhedron decreases by 0.7%, while the octahedral angular distortion OAV increases by 2.1%, i.e. the octahedra become more distorted towards low temperature. The behaviour of the Fe–Fe distances with T is of interest with respect to the magnetic ordering at low temperatures: the intra-chain distance decreases with temperature down to 30 K by ~0.23% (~0.008 Å), but seems to increase again below this temperature, a behaviour which is supported by the T-variation of the low T data, obtained from the Rietveld refinements (Fig. 4c). An increase of the M1–M1 distance within the octahedral M1 chain at low temperatures was also found in $CoGeO_3$ (Redhammer et al. 2009), in hedenbergite $CaFeSi_2O_6$ (Redhammer et al. 2008), or in $LiFeSi_2O_6$ (Redhammer et al. 2009) and can—in all cases—be associated with the magnetic ordering in the corresponding samples. The angle Fe–O1–Fe in $NaFeGe_2O_6$, involved in magnetic super-exchange between neighbouring Fe^{3+} sites within the M1-chain, decreases from 102.67(8)° towards low temperatures, however, the single-crystal neutron data reveal higher Fe–O–Fe angles of ~102.74(5)° at 30 K. Similar values were obtained from the Rietveld data, which suggest an increase from 102.73(8) at 20 K to 102.90(9)° at 5 K. These angles are well above the ideal 90° M1–O–M1 configuration that would favour a ferromagnetic coupling of spins. The shortest distance between two Fe^{3+} sites in different chains, $Fe–Fe_{inter}$, also decreases between room temperature and 30 K by similar absolute values of ~0.007(1) Å (~0.12%) as the intra-chain distances. The magnetic

super-exchange between neighbouring M1 chains involves the GeO_4: the super-super-exchange angles are Fe–O1–O2 and O1–O2–Fe with the larger O1–O2–Fe angle decreasing with decreasing temperature down to 100 K (Fig. 4d), but increasing again below 100 K. Data of the powder neutron measurements also display an increase of this angle down to the magnetic phase transition. The opposite effect is found for the smaller angle Fe–O1–O2 [114.12(5)° at 298 K], which increases towards 100 K, but decreases below this temperature (insert in Fig. 4d). A key point here is that the beginning magnetic ordering of the compound obviously alters or even reverses the *T*-variation of primary and secondary structural parameters far above the actual phase transition temperature, even if these changes are small but detectable with high resolution data. Given the delicate balance between competing magnetic interactions and the strong structure sensitivity of the interaction, even such small effects may have to be taken into account to reach a satisfactory theoretic description of these compounds.

The average Na–O bond length as well as the M2 polyhedral volume decrease with decreasing temperature, however, the neutron-diffraction data suggest that below 100 K both parameters increase again (Fig. 5). Among the individual Na–O bonds, the short Na–O3 bond remains almost constant between 2.5 and 298 K, while all other bond lengths decrease with decreasing temperature on similar scales. Below 100 K, the longer Na–O3 bonds, however, reverse their trends distinctly and increase to values similar to those at 298 K.

For the Ge–O bonds, only very small temperature variations can be estimated with all the individual and average Ge–O bonds increasing towards low temperature (0.002 Å on the average, Fig. 6). This is not unusual behaviour and was also found in $LiFeGe_2O_6$ (Redhammer et al. 2010b) and for aegirine itself (Fig. 6). Polyhedral

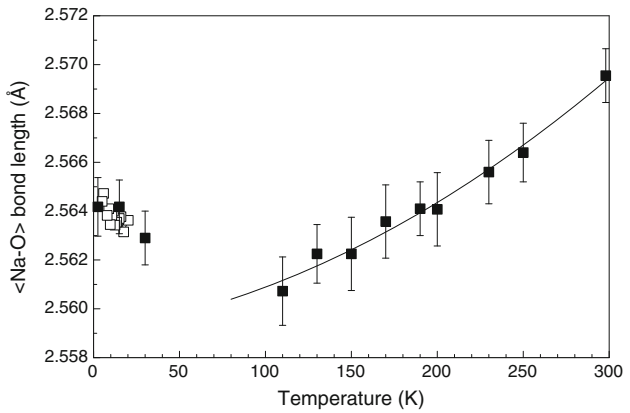

Fig. 5 Variations of the average Na–O bond lengths with temperature in $NaFeGe_2O_6$; *open symbols* are SPODI data, *curves* fitted to the data are guides to the eye only

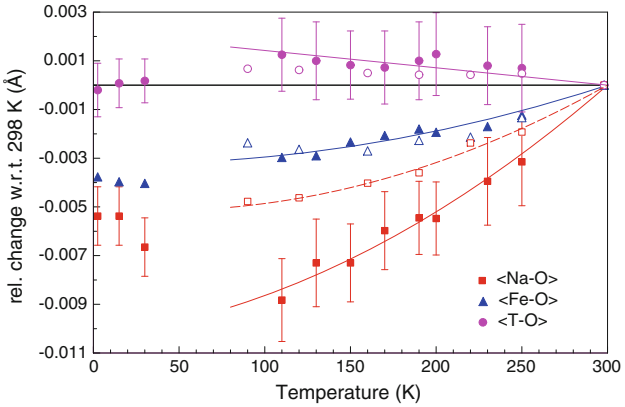

Fig. 6 Changes in mean bond lengths at the M2, M1 and T sites with respect to the values at 298 K; *filled symbols* are the data for $NaFeGe_2O_6$, *open symbols* the one for $NaFeSi_2O_6$. For the reason of clarity, *error bars* are shown for the <T–O> and <Na–O> data in the germanate only, *curves* fitted to the data are guides to the eye

distortion parameters remain constant, while the Ge–O3–Ge bonding angle decreases with temperature as does the O3–O3–O3 bridging-angle. Upon comparing the relative changes in volume and average bond lengths of the three building units M2 sites, M1 octahedra and Ge tetrahedra, the different thermal behaviour with decreasing temperature becomes evident: T polyhedra remain almost constant with *T*, while the M2 polyhedra distinctly shrink; the M1 polyhedra behave intermediate (Fig. 6). It is interesting to note that the thermal expansion of the T and M1 polyhedra is almost identical in $NaFeGe_2O_6$ and $NaFeSi_2O_6$, only the M2 sites expand more strongly in the germanate. Mechanisms need to be identified to account for the different thermal expansion of building units. One is the increased octahedral angular distortion, allowing a match between M1 and T sites but leaving bond lengths rather unchanged. Others can be found in the alteration of bond angles involving the tetrahedral sites. The decrease of the Ge–O–Ge bond angle expands the base plane of the tetrahedra, facilitating the match with the octahedral chain. Additionally, the O3–O3–O3 angle is lowered, i.e. the tetrahedral chains become more kinked towards lower *T*, which reduces their lateral dimension along the *c* axis. The increase in both angles below 100 K is probably a consequence of the increasing Fe–Fe separation within the M1 chain resulting from the increasing influence of the magneto-elastic coupling of Fe centres. The changes of the long Na–O3 bonds are directly coupled to the alterations in the O3–O3–O3 angles.

Bulk magnetic properties of $NaFeGe_2O_6$

The field dependence of the magnetization $M = f(H)$ was measured at 8.5, 19 and 32.5 K up to external fields of 55 kG. At all temperatures the susceptibility follows a

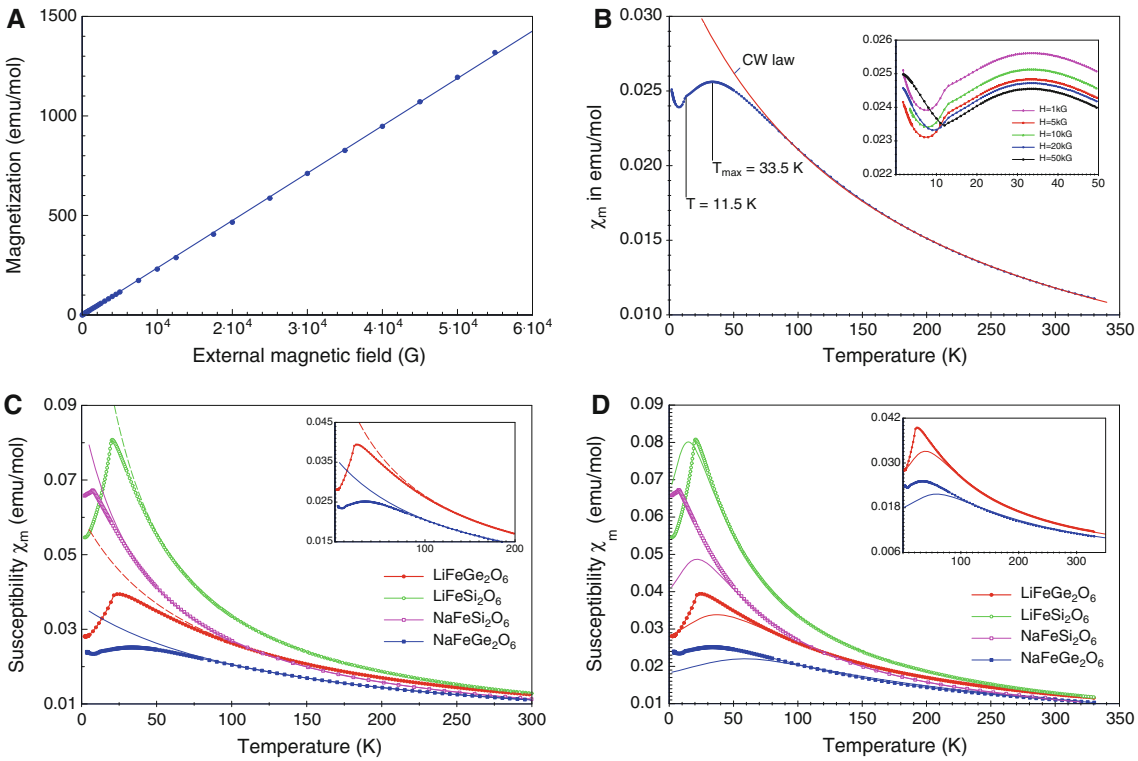

Fig. 7 Bulk magnetic measurements of polycrystalline $NaFeGe_2O_6$: **a** magnetization as a function of the external magnetic field at 8.5 K, **b** magnetic susceptibility at 1 kG, the *curve* fitted to the data corresponds to the Curie–Weiss law with $\chi = C_m/(T-\theta_P)$, the *inset* shows the temperature dependent susceptibility at different external fields with vanishing T_{kink} at 50 kG; **c** comparison for the magnetic susceptibilities of (Na,Li)Fe(Si,Ge)$_2O_6$ clinopyroxenes at 10 kG, *lines* fitted to the data correspond to the Curie-law, coefficients are given in Table 5, **d** as in **c**, but data are fitted to the Bonner–Fischer model (Bonner and Fischer 1964)

strictly linear magnetic field dependence (Fig. 7a). This is a similar behaviour to $NaFeSi_2O_6$, where the field dependency of the magnetization is also linear up to 55 kG (Baum et al. 1997), but distinctly different from the Li-bearing pyroxenes LiFe(Si,Ge)$_2O_6$, where spin-flop transitions were found above 40 kG (Redhammer et al. 2009).

The magnetic susceptibility χ_{molar} of synthetic $NaFeGe_2O_6$ at an external field of 1 kG displays a broad maximum at 33.5(3) K and a drop in the susceptibility around 11.5(2) K (Fig. 7b). Above 100 K, the inverse magnetic susceptibility $1/\chi_{molar}$ can be fitted with a Curie–Weiss law, from which the paramagnetic Curie temperature Θ_P is determined to be −154.6(5) K, the experimental magnetic moment $\mu_{CW} = 6.55(5)\mu_B$. This strongly negative paramagnetic Curie temperature suggests dominating AFM coupling in $NaFeGe_2O_6$. The position of the peak susceptibility T_{max} remains constant at 33.5(3) K with increasing external field up to 50 kG, as does the position of the low temperature kink in χ at $T_{kink} = 11.5(3)$ K. This latter kink is no longer observed at 50 kG, which could be seen as an indication that the magnetic structure is modified/destroyed by external fields. The paramagnetic Curie temperature decreases with increasing external field up to values of −114 K at 20 kG, while the experimental magnetic moment μ_{CW} approaches the theoretical spin only value of $5.92\mu_B$ for Fe^{3+}. For comparison, the susceptibility of a synthetic aegirine $NaFeSi_2O_6$, sample Ac#24 of Redhammer et al. (2000) was measured also. Aegirine shows a low ordering temperature of $T_N = 7.8$ K, a slight change in slope is observable around 6.4 K (point of inflection). From the inverse magnetic susceptibility a negative paramagnetic Curie temperature of $\Theta_P = -43.6$ K was obtained with $\mu_{CW} = 5.56(5)\mu_B$. These data are in good agreement with data from literature, e.g. Baum et al. (1997). Recently, Jodlauk et al. (2007) presented a temperature versus external magnetic field phase diagram (their Fig. 3), where it is stated that $NaFeSi_2O_6$ possesses a collinear spin structure between 8 and 6 K, while below 6 K it transforms to a ferroelectric phase with the magnetic ordering likely to be helical and incommensurate (Jodlauk et al. 2007).

Among all the alkali-iron clinopyroxenes, $NaFeGe_2O_6$ has the strongest negative Θ_P (Table 5) and also the largest difference between T_{max} and T_N. Also it is evident from Fig. 7c and Table 5, that $NaFeGe_2O_6$ exhibits the broadest maximum in χ, followed by $LiFeGe_2O_6$; Those are the two compounds which have the largest chain-to-chain separation among the four clinopyroxenes (Table 4), while

Table 5 Bulk magnetic properties of the alkali-iron clinopyroxenes at an external field of 10 kG

Sample	T_{max}	T_N	θ_P	C_m	μ_{CW}	$T_{max}-T_N$	J/k	Ref
LFS	20.6	18.3	−25.4	4.125	5.74	2.3	−1.6	(b)
NFS	7.8	6.7	−43.6	3.859	5.56	1.1	−2.8	(a)
LFG	24.4	20.2	−78.6	4.744	6.16	4.2	−4.5	(b)
NFG	33.8	11.2	−131.8	4.773	6.18	22.6	−7.0	(a)

T_N Neel temperature (K), θ_P paramagnetic Curie temperature (K), C_m Curie constant, μ_{CW} experimental magnetic moment from Curie–Weiss fit (μ_B), J/k exchange coupling constant

[a] this study

[b] Redhammer et al. (2009)

$LiFeSi_2O_6$ has the smallest one and displays the sharpest maximum in χ. From this, it is concluded that $NaFeGe_2O_6$ has the most pronounced 1D character among the Fe^{3+} pyroxenes but finally transforms to a 3D anti-ferromagnetically ordered state at some lower temperatures, while $LiFeSi_2O_6$ is the most ideal one in terms of a 3D ordered structure.

As a distinctly low-dimensional character is present, especially in the germanium clinopyroxenes under investigation; we applied the Bonner–Fisher model (Bonner and Fischer 1968) according to:

$$\chi_{chain} = \frac{N_B g^2 \beta^2 S(S+1)}{3k_b T} \cdot \frac{1+v}{1-v}$$

and

$$v = \coth\left[\frac{2JS(S+1)}{k_b T}\right] - \frac{k_b T}{[2JS(S+1)]}$$

with $g = 2.0$, $S = 5/2$ and $N =$ Avogadro number. We estimated the inter-chain coupling constants J/k by fitting this quantity to the experimental data. Although the fit of the Bonner–Fischer model deviates significantly from the experimental data at low temperatures (Fig. 7d), the data evaluation shows—at least semi-quantitatively—that in $NaFeGe_2O_6$ the intra-chain coupling constant is largest with $J/k \sim -7.0$, thus anti-ferromagnetic, while it is −1.6 in $LiFeSi_2O_6$ (Table 5). The latter compound shows the limitation of the applicability of model as the actual magnetic ground state in $LiFeSi_2O_6$ is ferromagnetic within the chain, although the paramagnetic Curie temperature indicates a dominating AF-interaction at higher temperatures (Redhammer et al. 2009). More advanced models would have to be applied to better describe the susceptibility data of the alkali-iron clinopyroxenes including also the significant inter-chain coupling; the Bonner–Fischer model, assuming simple isotropic 1D-Heisenberg chains gives qualitative estimates of the coupling constants only. Nevertheless, the intra-chain coupling appears to be stronger in the germanate compounds, with sodium on M2 dominating over Li. The inter-chain coupling becomes dominating in $LiFeSi_2O_6$ (Redhammer et al. 2009).

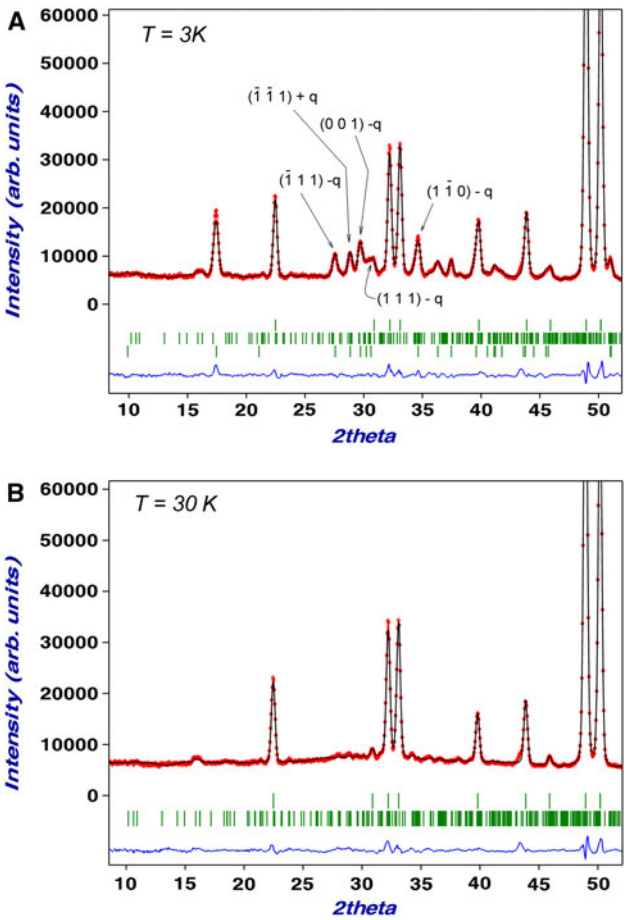

Fig. 8 Low angle parts of the neutron diffraction pattern of $NaFeGe_2O_6$ (λ = 2.537 Å), collected at 30 and 3 K at the SPODI diffractometer; the *tick marks* show the position of the nuclear (*upper*) and the magnetic (*lower*) Bragg-peaks, the *middle tick marks* corresponds to the 3% $^{\lambda}/_{3}$ contamination of neutron beam; indices of some selected magnetic peaks are given with $\mathbf{q} = \mathbf{k} =$ (0.3230, 1, 0.0802)

Magnetic spin structure of $NaFeGe_2O_6$

Neutron-diffraction measurements, performed on the powder sample between 20.2 and 13.4 K, show Bragg peaks resulting from the nuclear structure only. The data can be indexed and refined on the basis of the monoclinic *C*2/*c* structure. Additional Bragg contributions start to appear at 12.5 K, resulting from the 3-dimensional magnetic ordering of the sample and quickly gain intensity towards lower temperatures (Fig. 8).

Indexing of these additional peaks was not possible with any commensurate propagation vector, i.e. tests with $\mathbf{k} =$ (1 0 0), (0 1 0), (0 0 0) or any simple doubling of the magnetic unit cell failed. Also it was not possible to

refine the magnetic contributions with the k-vector of $\mathbf{k} = (k = 0, 0, 1/2)$ as proposed by Behruzi et al. (1997). Thus, the peak positions of the magnetic satellite reflections were carefully determined using the peak-fitting tool in "winplotr", afterwards the program "k-search" was used to find possible incommensurate propagation vectors (both programs are part of the FULLPROF-SUITE, Rodríguez-Carvajal 2001). Assuming the *C*2/*c* symmetry, the magnetic reflections could finally be modelled with an incommensurate k-vector $\mathbf{k} = (0.32, 1.0, 0.08)$, which refined to $\mathbf{k} = [0.3230(5), 1.0, 0.0802(2)]$ at 5 K in subsequent profile matching refinements. All magnetic satellite reflections and shoulders could be matched with this **k**-vector. As single crystals became available during the course of this study, a data collection at 4 K was done at the RESI-diffractometer (FRM II) using an image plate diffractometer to validate this **k**-vector. From this data, the propagation vector which was refined to $\mathbf{k} = [0.3220(3), 1.0003(4), 0.0806]$, thus being in perfect agreement with the one extracted from the powder data. The magnetic propagation vector does not remain constant but is temperature dependent; both $\mathbf{k_x}$ and $\mathbf{k_z}$ decrease with increasing temperature, with $\mathbf{k_x}$ decreasing more strongly (Fig. 9). However, no special values for any component are reached, even if $\mathbf{k_x}$ approaches 1/3 at low temperatures, but do not reach it.

The determination and refinements of the incommensurably modulated magnetic structure was done using irreducible representational analysis. Possible spin arrangements, compatible with space group *C*2/*c* were calculated with the programs BasiReps (Rodríguez-Carvajal 2001) and SARA*h* (Wills 2000). For $\mathbf{k} = (0.323, 1.0, 0.080)$, the decomposition of the magnetic representation for Fe^{3+} on the 4*e* site is $\Gamma_{mag} = 3\Gamma_1 + 3\Gamma_2$, yielding two basic functions of the irreducible representations, namely:

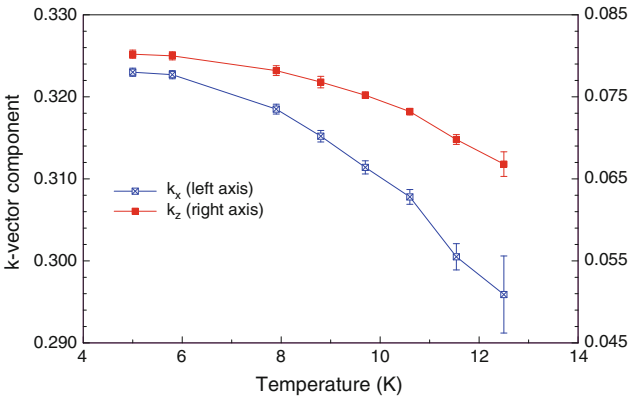

Fig. 9 Variation of the incommensurate propagation vector k with temperature for $NaFeGe_2O_6$ as determined from the Rietveld refinements of powder data

$$\text{IReps1} : \text{Fe\_2} = (u, v, w) \text{ and Fe\_2} = (r_0 - i \times r_1) \times (-u, v, -w),$$

$$\text{IReps2} : \text{Fe\_1} = (u, v, w) \text{ and Fe\_2} = (r_0 - i \times r_1) \times (u, -v, w),$$

with $r_0 = 0.9685$ and $r_1 = 0.2486$ for Fe_1 on (0, *y*, 1/4) and Fe2_2 on $(0, -y + 1, 3/4)$ with $y = 0.9038$, respectively. Each representation has 3 degrees of freedom for the components of the magnetic moment of iron $\mathbf{m_x}$, $\mathbf{m_y}$ and $\mathbf{m_z}$, yielding a sine-modulation, while three more degrees of freedom, representing the imaginary parts of $\mathbf{m_x}$, $\mathbf{m_y}$ and $\mathbf{m_z}$ have to be considered, if a helical spin structure is assumed. Rietveld refinements on the powder-diffraction data, collected at 5 K, quickly showed that only with IReps1, a satisfying refinement of the data can be obtained and further it turned out that a helical modulation of spins gives significantly lower agreement indices compared to a model with sine-modulation. The spin structure, obtained from the powder data at 5 K, was successfully verified using the 2.5 K single-crystal neutron data. Below the single-crystal data will be discussed.

$NaFeGe_2O_6$ posses an incommensurately modulated helical spin structure. The magnetic spins lie in the **a**–**c** plane, no significant magnetic moment $\mathbf{m_y}$ is observed along the *b* axis. Within a M1 chain, the magnetic spins are anti-ferromagnetically coupled, but canted relative to each other from spin to spin along the *c* axis with a rotation of 360°, after approximately 26 spins (Fig. 10a–c). Along the *c* axis, the incommensurately modulation amounts 25 unit cell, i.e. a spin has the same orientation after ~137.8 Å, while along the *a* axis a similar orientation is found after ~33 times the *a* axis, i.e. after ~329.8 Å. Along the *b* axis, no incommensurate modulation is present and the repeat unit exactly is the 8.8629 Å (Fig. 10b). Spins in two neighbouring M1 chains, which interact via super-super-exchange along the short inter-chain distance of ~5.64 Å (J_1 in Fig. 2 and red lines in Fig. 10b) are rotated away from each other by an angle of $\delta \sim 68°$–$78°$, i.e. they have no parallel spin orientation. Rotating one spin relative to the other by this angle δ would result in a ferromagnetic coupling of the spins between the M1 chains. This would correspond to a spin arrangement, which is found e.g. between the M1 chains, coupled via the GeA tetrahedra in $LiFeGe_2O_6$ (Redhammer et al. 2009) or which was proposed for $NaFeSi_2O_6$ by Ballet et al. (1989). Rotating by 180-δ would result in a situation, which was found between the M1 chains in $LiFeGe_2O_6$ which are coupled via the GeB super-exchange. Concluding $NaFeGe_2O_6$, which has only one distinct tetrahedral chain (due to the *C*2/*c* symmetry), shows a frustrated spin arrangement, intermediate between the alternating FM and AFM coupling in $LiFeGe_2O_6$.

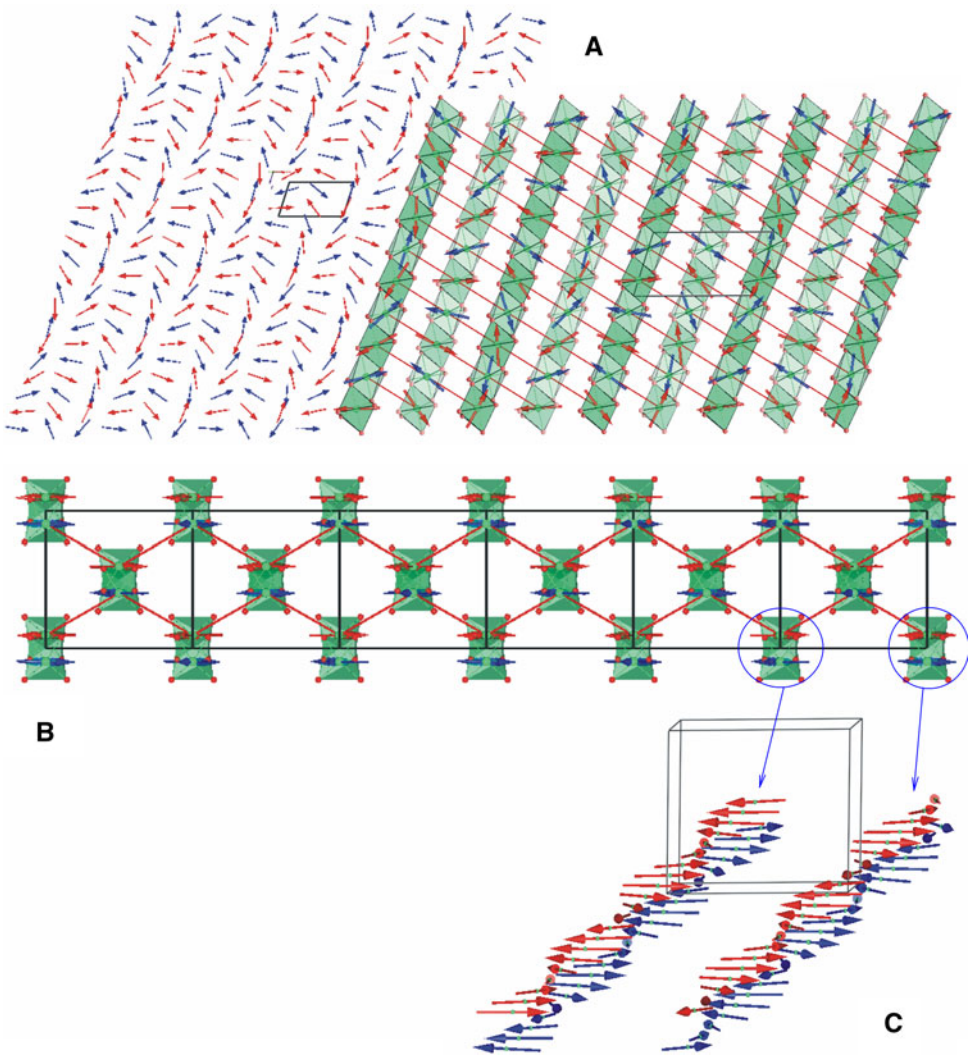

Fig. 10 Scheme of the magnetic structure of $NaFeGe_2O_6$ at 2.5 K as determined from single-crystal neutron diffraction data. Magnetic spins of neighbouring Fe^{3+} atoms within the M1 chain are shown in *blue* (Fe_1 = 0, *y*, 0.25) and *red* (Fe_2 = 0, $-y+1$, 0.75) to highlight the anti-ferromagnetic coupling within the M1 chains but belong to the same magnetic lattice; **a** is a projection along (1 0 0), **b** is a projection along **c*** and **c** is a 3-dimensional view depicting the helical nature of spins along the *c* axis

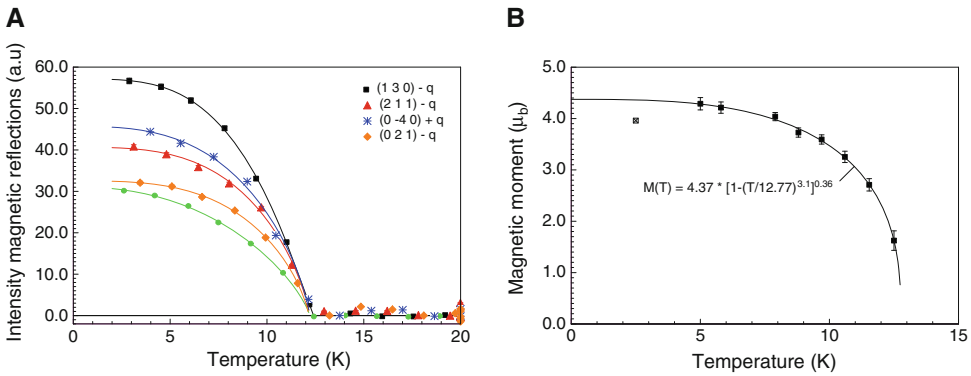

Fig. 11 **a** Intensity decay of selected magnetic reflections and **b** variation of the magnetic moment with temperature. *Lines* fitted to the data correspond to a phenomenological power law as described in the text

The intensity decay with increasing temperature of selected magnetic reflections, collected on the single crystal, was fitted to a phenomenological power law, including ordering temperature and critical exponent β (Fig. 11a). These data suggest a magnetic ordering temperature of ~12.4–12.9 K, which agrees very well with the temperature at which the low temperature kink in the susceptibility data was observed. The critical exponents are in the range of $\beta = 0.38$–0.45. At 2.5 K the total magnetic moment at the Fe site (x, y, z) is 4.09(4)μB. This is a somewhat smaller magnetic moment than the one obtained from the powder data, where 4.29(9) μB were found at 5 K. However, it has to be noted that in the powder data the helical model yield a small component up to 0.4 μ_B along

the *b* axis, which could not be verified by the single-crystal data but contributes to the total magnetic moment. The variation of the magnetic moments, obtained from the Rietveld refinements with temperature (Fig. 11b) was fitted with a phenomenological power law as given by Blundell et al. (2003) with $M(T) = M(0)*[1-(T/T_N)^{\alpha}]^{\beta}$, yielding $T_N = 12.77(9)$, $\alpha = 3.1(3)$, and $\beta = 0.36(3)$. The critical exponent β is consistent with a 3D model of ordering ($\beta_{ideal} = 0.367$ and 0.326 for a 3D-Heisenberg or a 3D-Ising model, respectively).

New data on the magnetic structure of $NaFeSi_2O_6$ (aegirine)

Additionally, to the title compound a powder sample of synthetic aegirine, produced by a ceramic sintering technique as described in "Material synthesis", was studied by neutron-diffraction at 5 and 12.5 K using 2.537 Å SPODI data. Unfortunately, only a sample diluted with 23.5 wt.% SiO_2 and 8.3 wt.% Fe_2O_3 was available. We observe magnetic ordering of $NaFeSi_2O_6$ between the two temperatures as is evident by the appearance of well-resolved magnetic reflections at 15.8° and 16.6° and 36.3° 2θ, additionally prominent broad peaks around 20.7° and 38.5° are present at 5 K (Fig. 12a); very similar observations were made by Ballet et al. (1989) in their neutron-diffraction study on aegirine. The prominent reflections at 15.78 and 16.62° 2θ are similar to the ones observed in $LiFeSi_2O_6$ and can be indexed as (1 0 0) and (0 1 0) on basis of a commensurate propagation vector with $\mathbf{k} = (1, 0, 0)$. However, with this and any other commensurate k-vectors it was not possible to index the broad peaks around 20.7° and 38.5°, and also the doublet around 16° reveals some small shoulders, indicative that the magnetic ordering in $NaFeSi_2O_6$ is incommensurate (Fig. 12a). In a first step of evaluation, we searched for an incommensurate propagation vector by which all magnetic reflections could be matched. This was only possible assuming *P*-1 symmetry yielding $\mathbf{k} = (0.58, 0.53, 0.49)$. However, using this propagation vector in magnetic structure solution the strong intensities at 15.78 and 16.62° 2θ could not be modelled with any spin configuration tested.

Based on the arguments of Jodlauk et al. (2007), who state that a commensurate magnetic structure for aegirine is stable between 8 and 6 K, but transforms to an incommensurate modulated one below 6 K, we propose that in

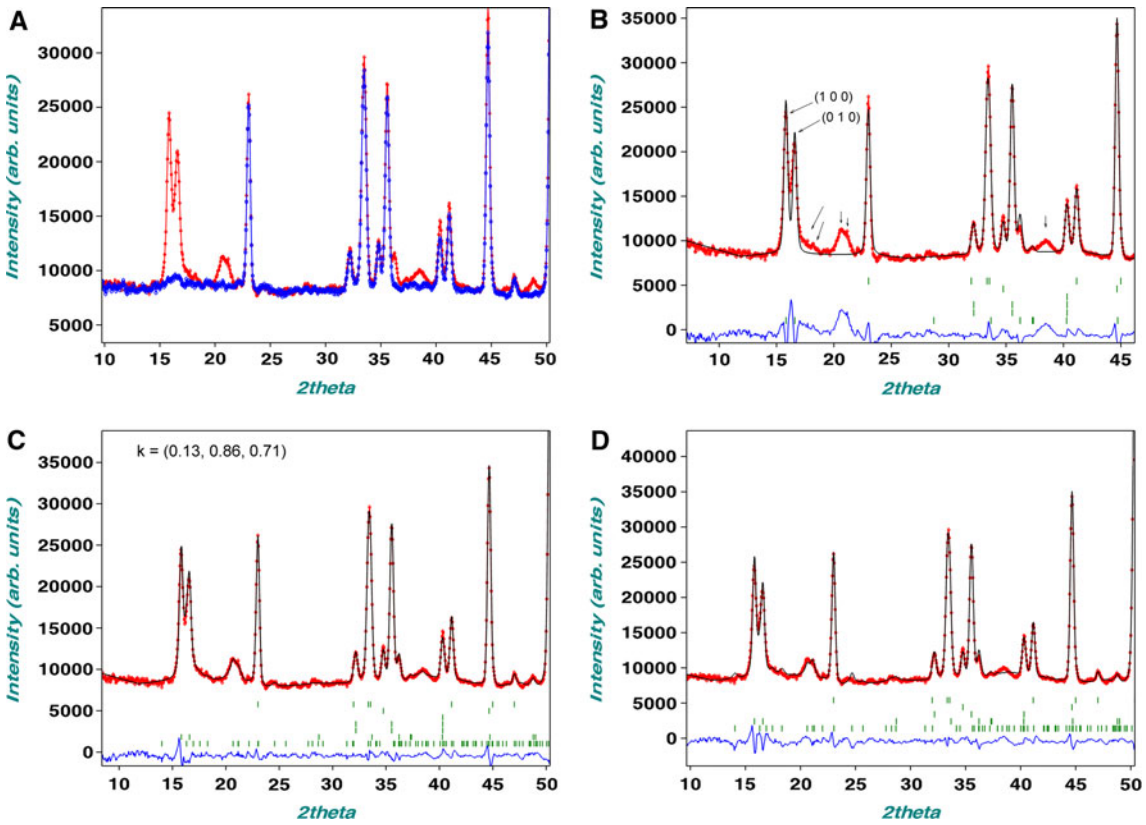

Fig. 12 Low angle parts of the neutron diffraction pattern of $NaFeSi_2O_6$ ($\lambda = 2.537$ Å), collected at the SPODI diffractometer. **a** Comparison between 12.5 K (*blue*) and 5 K (*red*) data, additional magnetic reflections are evidently visible, **b** 5 K data evaluated with a commensurate model of the magnetic spin structure only, **c** 5 K data evaluated using the commensurate model of (**b**) and pattern matching for the incommensurately modulated phase, **d** 5 K data evaluated with a commensurate and an incommensurate model of ordering

our sample at 5 K (and obviously also in the 1.4 K measurement of Ballet et al. 1989) both magnetic phases are present: the commensurate structure is preserved at 5 K in the powder data and additionally an incommensurately modulated phase of aegirine appears which probably is stable towards lower temperatures. In a second step of evaluation, the magnetic structure of the commensurate phase was solved using representational analysis assuming $\mathbf{k} = (1, 0, 0)$ and $C2/c$ symmetry. The only spin configuration, which can adequately describe the doublet at low angles is the configuration having (u, 0, w) and (u, 0, w) for Fe_1 and Fe_2 on (x, y, z) and $(-x,-y + 1,-z + 1)$, respectively, the resulting magnetic space group is $C2'/c'$, with $R_{\mathrm{Mag}} = 3.9\%$ (Fig. 12b). This is the same magnetic symmetry as observed in monoclinic $CoGeO_3$ (Redhammer et al. 2010a) or in $CaCoGe_2O_6$ (Redhammer et al. 2008). The model for $NaFeSi_2O_6$ gives components of the magnetic moment $\mathbf{m_x} = 1.01(7)\mu_B$ and $\mathbf{m_z} = 2.46(2)\mu_B$, resulting in a total magnetic moment of $2.37\mu_B$. This value is distinctly smaller than the theoretical spin only moment of Fe^{3+} of $5.92\mu_B$, indicating that ordering is not saturated or highly frustrated. The magnetic spins lie within the **a**–**c** plane, forming an angle of 84(1)° with the a axis; the coupling of spins is FM within the M1 chains, but AFM between neighbouring chains (Fig. 13a). Similar spin configurations are found in $LiFeSi_2O_6$ (Redhammer et al. 2009) or in $NaCrGe_2O_6$ (Nenert et al. 2009a, b). These observations are in good agreement with single-crystal magnetization measurements on an natural aegirine of Baum et al. (1997), who found the easy axis for the magnetization to lie within the **a**–**c** plane, forming an angle of 50(2)° with the a axis.

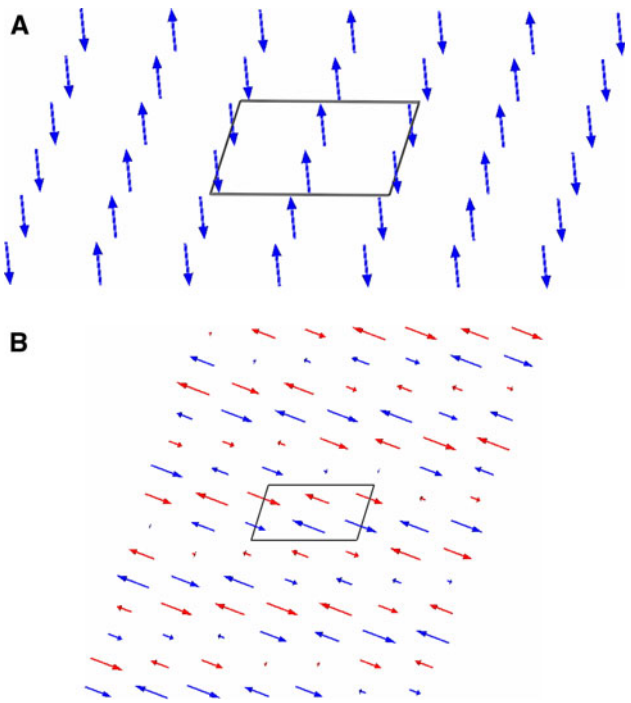

Fig. 13 Schemes of the magnetic structures of $NaFeSi_2O_6$ (aegirine) at 5 K as determined from powder neutron diffraction data. **a** Model for the commensurate structure with $\mathbf{k} = (1, 0, 0)$ and $C2'/c'$ symmetry in a projection onto the (1 0 1) plane, **b** model of the incommensurately modulated structure with spin density waves within the (1 0 1) plane

Using only incommensurate satellite reflections, taking into account a distinct shoulder at 16.3° 2θ within the (1 0 0)/(0 1 0) doublet and assuming the broad peak at 20.7° being composed out of two reflections at least, a possible propagation vector $\mathbf{k} = [0.1335(8), 0.855(1), 0.708(1)]$ was determined in C-1 symmetry (Fig. 12c). In order to keep refinement parameters low due to the limited number of observations, it had to be assumed that the magnetic moments at the Fe sites are collinear. Doing so, the refinement quickly converged to a spin structure with $\mathbf{m_x} = 2.59(4)$, $\mathbf{m_y} = 0.31(6)$, $\mathbf{m_z} = 2.84(4)\mu_B$ and $R_{\mathrm{mag}} = 6.7\%$ (Fig. 12d), describing a longitudinal spin density wave mostly oriented within the **a**–**c** plane. The maximum magnetic moment within this wave is $\sim$3.3 μB, the spins form an angle of $\sim$21° with the a axis. Within the spin density wave, magnetic moments are ferromagnetically coupled but change orientation every $\lambda/2$ (Fig. 13b). Any attempts to refine also the imaginary parts of the magnetic moments resulted in sever convergence problems; also it was not possible to refine the magnetic moments on the different Fe site independently. So, we cannot finally decide if the magnetic structure of aegirine has helical order or better is described by a spin density wave as done here.

Conclusion

The germanate analogue to aegirine, $NaFeGe_2O_6$, adopts the well known HT-$C2/c$ clinopyroxene structure at room temperature, and retains this symmetry down to 2.5 K. Some key features of the structure are the almost stretched tetrahedral chains and large Fe–Fe interatomic separations, within and between neighbouring M1 chains. These large distances between Fe^{3+} atoms are possibly responsible for the lower magnetic ordering temperature compared to $LiFeGe_2O_6$.

Below 12 K, $NaFeGe_2O_6$ transforms to a 3-dimensionally magnetically ordered state, however, ordering is incommensurately modulated. The chain to chain coupling cannot be assigned as pure FM or AFM. The spins, interacting by super-super-exchange via the GeO_4 tetrahedra, are rotated relative to each other by $\sim$70–80°. This represents an intermediate state to what is found in $LiFeGe_2O_6$. In this clinopyroxene, with lower space group symmetry $P2_1/c$, there are two symmetrically distinct tetrahedral chains; the

intra-chain spin interaction is AFM, but the inter-chain coupling alternates between FM and AFM, causing a doubling of the magnetic unit cell along the *a* axis.

The magnetic ordering temperature $T_N = 12.8$ K, obtained from the neutron-diffraction data (intensity data and *T*-variation of the magnetic moment), agrees with the low temperature kink in the magnetic susceptibility data. It is concluded, that the peak susceptibility at $T_{max} \sim 33.5$ K may correspond to the beginning of low dimensional magnetic ordering (1D or 2D), while a 3D incommensurate ordering sets on at 12.8 K. Among the alkali-iron clinopyroxene series, $NaFeGe_2O_6$ displays the most distinct quasi 1D-character (broad maximum in the susceptibility, large chain separation), even though there is a pronounced inter-chain coupling. The helical magnetic spin structure of $NaFeGe_2O_6$ makes this compound to be a promising candidate for multiferroic behaviour.

The analogue silicate aegirine, $NaFeSi_2O_6$, orders magnetically at temperatures below 8 K. Its magnetic structure is described by two different spin-structures: (1) a commensurate and collinear one with $\mathbf{k} = (1, 0, 0)$ and $C2'/c'$ symmetry having the spins ferromagnetically coupled within a M1 chain and oriented at 84° to the *a* axis, and (2) an incommensurately modulated structure, best being described by a spin density wave, which is oriented within (1 0 1), being only slightly tilted out of this plane. Following the results of Jodlauk et al. (2007), the commensurate structure might be stable between 8 and 6 K, while the incommensurate structure appears below 6 K, associated with the onset of ferroelectricity (Jodlauk et al. 2007). However, the commensurate structure seems to be preserved meta-stably down to 1.4 K (Ballet et al. 1989). Some more detailed investigations in the temperature range 10–0.5 K, on phase pure powder samples and single crystals, are necessary to fully understand the magnetic phase transitions and phase relations in aegirine, and are part of our ongoing studies on the magnetic properties of pyroxenes.

Acknowledgment This work was supported by the Fonds zur Förderung der wissenschaftlichen Forschung, FWF, Vienna under grants number R33-N10 and P19762/N10. Neutron-diffraction experiments have been supported by the European Commission under the 7th Framework Programme through the "Research Infrastructures" action of the "Capacities" Programme, Contract No: CP_CSA_Infra-2008-1.1.1 Number 226507-NIMI3. We would like to thank F. Cámara and an anonymous referee for their helpful comments on the manuscript.

References

Ballet O, Coey JMD, Fillion G, Ghose A, Gewart A, Regnard JR (1989) Magnetic order in acmite; $NaFeSi_2O_6$. Phys Chem Miner 16:672–677

Baum E, Treutmann W, Lottermoser W, Amthauer G (1997) Magnetic properties of the clinopyroxenes aegirine and hedenbergite: a magnetic susceptibility study on single crystals. Phys Chem Miner 24:294–300

Behruzi M, Schäfer W, Kockelmann W, Tietze-Jaensch H (1997) Magnetic structure of the pyroxene $NaFeGe_2O_6$. ISIS Experimental Report #9079, Rutherford Appleton Laboratory (http://www.isis.rl.ac.uk/isis97/reports/9079.pdf)

Blundell SJ, Steer CA, Pratt FL, Marshall IM, Hayes W, Ward RCC (2003) Detection of magnetic order in the S = 1 chain compound $LiVGe_2O_6$ using implanted spin-polarized muons. Phys Rev B67:224411 (4 pages)

Bonner JC, Fischer ME (1968) Linear magnetic chains with anisotropic coupling. Phys Rev 135:A640–A658

Bruker-Nonius (2004) APEX2: software suite for data collection and processing of single crystal X-ray diffraction data. Bruker AXS Inc, Madison

Downs RT (2005) XtalDraw for Windows. Commission on Powder Diffraction, IUCr Newsletter 30:32–33

Drokina TV, Bayukov OA, Petrakovskii GA, Velikanov DA, Bovina AF, Stepanov GN, Ivanov DA (2008) Synthesis and properties of $NaFeGe_2O_6$ polycrystals. Phys Solid State 50(11):2141–2144

Duisenberg AJM (1992) Indexing in single-crystal diffractometry with an obstinate list of reflections. J Appl Crystallogr 25:92–96

Duisenberg AJM, Kroon-Batenburg LMJ, Schreurs AMM (2003) An intensity evaluation method: EVAL-14. J Appl Crystallogr 36:220–229

Farrugia L (1999) WinGX suite for small-molecule single-crystal crystallography. J Appl Crystallogr 32:837–838

Hoelzel M, Senyhyn A, Gilles R, Boysen H, Fuess H (2007) The strutcure powder diffractometer SPODI. Neutron News 18(4): 23–26

Jodlauk S, Becker P, Mydosh JA, Khomskii DI, Lorenz T, Streltsov SV, Hezel DC, Bohaty L (2007) Pyoxenes: a new class of multiferroics. J Phys Condens Matters 19(43):432201 (9 pp)

Nenert G, Isobe M, Ritter C, Isnard O, Vasiliev AN, Ueda Y (2009a) Magnetic and crystal structure of the magnetoelectric pyroxene $LiCrSi_2O_6$. Phys Rev B79:064416 (8 pp)

Nenert G, Ritter C, Isobe M, Isnard O, Vasiliev AN, Ueda Y (2009b) Magnetic and crystal structures of the one-dimensional ferromagnetic chain pyroxene $NaCrGe_2O_6$. Phys Rev B80:024402 (7 pp)

Redhammer GJ, Amthauer G, Lottermoser W, Treutmann W (2000) Synthesis and structural properties of clinopyroxenes on the hedenbergite $CaFe^{2+}Si_2O_6$–aegirine $NaFe^{3+}Si_2O_6$ solid solution. Eur J Mineral 12(1–2):105–120

Redhammer GJ, Roth G, Paulus W, André G, Lottermoser W, Amthauer G, Treutmann W, Koppelhuber-Bitschnau B (2001) Crystal and magnetic structure of Li–Aegirine $LiFe^{3+}Si_2O_6$: a temperature dependent study. Phys Chem Miner 28:337–346

Redhammer GJ, Amthauer G, Roth G, Tippelt G, Lottermoser W (2006) Single crystal X-ray diffraction and temperature dependent 57Fe Mössbauer spectroscopy of the hedenbergite–agirine (Ca, Na)(Fe^{2+}, Fe^{3+})Si_2O_6 solid solution. Am Mineral 91(7–8):1271–1292

Redhammer GJ, Roth G, Treutmann W, Paulus W, André G, Pietzonka C, Amthauer G (2008) Magnetic ordering and spin structure in Ca-bearing clinopyroxenes $CaM^{2+}(Si, Ge)_2O_6$, M = Fe, Ni, Co, Mn. J Solid State Chem 181:3163–3176

Redhammer GJ, Roth G, Treutmann W, Hoelzel M, Paulus W, André G, Pietzonka C, Amthauer G (2009) The magnetic structure of clinopyroxene-type $LiFeGe_2O_6$ and revised data on multiferroic $LiFeSi_2O_6$. J Solid State Chem 182:2374–2384

Redhammer GJ, Senyshyn A, Tippelt G, Pietzonka C, Roth G, Amthauer G (2010a) Magnetic and nuclear structure and thermal

expansion of orthorhombic and monoclinic polymorphs of $CoGeO_3$ pyroxene. Phys Chem Miner 37(5):311–332

Redhammer GJ, Cámara F, Alvaro M, Nestola F, Tippelt G, Prinz S, Simons J, Roth G, Amthauer G (2010b) Thermal expansion and high temperature $P2_1/c$–$C2/c$ phase transition in clinopyroxene-type $LiFeGe_2O_6$ and comparison to $NaFe(Si,Ge)_2O_6$. Phys Chem Miner (http://dx.doi.org/10.1007/s00269-010-0368-1)

Renner B, Lehmann G (1986) Correlation of angular and bond lengths distortion in TO_4 units in crystals. Z Kristallogr 175:43–59

Robinson K, Gibbs GV, Ribbe PH (1971) Quadratic elongation, a quantitative measure of distortion in polyhedra. Science 172: 567–570

Rodríguez-Carvajal J (2001) Recent developments of the program. Commission on Powder Diffraction (IUCr) Newsletter 26, 12–19. (http://journals.iucr.org/iucr-top/comm/cpd/Newsletters/)

Solov'eva LP, Bakakin VV (1968) X-ray study of the sodium-iron metagermanate $NaFeGe_2O_6$. Sov Phys Crystallogr 12(4): 517–520

Streltsov SV, Khomskii DI (2008) Electronic structure and magnetic properties of pyroxenes (Li, Na)TM(Si, $Ge)_2O_6$: low-dimensional magnets with 90° bonds. Phys Rev B77:064405 (11 pp)

Vasiliev AN, Ignatchik OL, Sokolov AN, Hiroi Z, Isobe M, Ueda Y (2005) Long-range magnetic order in quasi-one-dimensional chromium-based ($S = 3/2$) pyroxenes $(Li,Na)Cr(Si,Ge)_2O_6$. Phys Rev B 72:012412 (4 pp)

Wills AS (2000) A new protocol for the determination of magnetic structures using simulated annealing and representational analysis (SARAh). Physica B Cond Matter 276–278:680–681